A Mouse Model of Rett Syndrome shows a Cell-Autonomous Reduction of α4* Nicotinic Receptors in Dopaminergic Neurons of the Substantia Nigra Pars Compacta

by

Keyrian L. Le Gratiet

A THESIS SUBMITTED IN PARTIAL FULFILMENT
OF THE REQUIREMENTS FOR THE DEGREE OF
BACHELOR OF SCIENCE (HONS.)
In the Department of
BIOLOGY,
UNIVERSITY OF VICTORIA

_____
Dr. Kerry Delaney

_____
Dr. Raad Nashmi

_____
Dr. John Taylor

_____
Dr. Robert Chow

Honours Committee

A Mouse Model of Rett Syndrome shows a Cell-Autonomous Reduction of α4* Nicotinic Receptors in Dopaminergic Neurons of the Substantia Nigra Pars Compacta

by

Keyrian L. Le Gratiet

Honours Committee

Dr. Kerry Delaney, Department of Biology
Co-supervisor

Dr. Raad Nashmi, Department of Biology
Co-supervisor

Dr. John Taylor, Department of Biology
Honours Program Supervisor

Dr. Robert Chow, Department of Biology
Departmental member

Abstract

Honours Committee

Dr. Kerry Delaney, Department of Biology
Co-supervisor

Dr. Raad Nashmi, Department of Biology
Co-supervisor

Dr. John Taylor, Department of Biology
Honours program supervisor

Dr. Robert Chow, Department of Biology
Departmental member

Rett syndrome (RTT) is a neurodevelopmental disorder due to spontaneous mutations in a gene (*MECP2*) on the X chromosome. With the mutations typically found in the paternal germline, female RTT patient are more common than males and manifest a constellation of severely debilitating symptoms after birth. Development is mostly normal during the first 6 months but then stalls and regresses resulting in individuals that lack motor coordination, have impaired speech, and exhibit Parkinsonian symptoms often accompanied by seizures. Mice with the same mutation have many neuronal dysfunctions including poor neural communication, some of which is due to improper signaling by the transmitter acetylcholine (ACh). The cholinergic system is critically involved in the generation of purposeful behaviours including voluntary motor acts, which correlate with some of the conditions seen in RTT patients.

The present study investigated whether mutant ($Mecp2^{-}$) dopaminergic (DAergic) cells have downregulated α4-containing (α4*) nicotinic acetylcholine receptor (nAChRs) expression compared to wild-type (Wt) ($Mecp2^{+}$) DAergic cells in the substantia nigra pars compacta (SNc) of a RTT female mouse and whether this downregulation was cell-autonomous. Spectral confocal imaging was used to quantify the YFP-tagged α4* nAChRs in five-week-old $Mecp2^{EGFP/+}/\alpha4^{YFP/+}$, $Mecp2^{+/-}/\alpha4^{YFP/+}$, and $Mecp2^{+/+}/\alpha4^{YFP/+}$ female mice.

Imaging confirms that mutant DAergic neurons have reduced expression of α4* nAChRs compared to spatially colocalized Wt DAergic neurons in the SNc of a young RTT female mouse. Furthermore, the reduction in nAChR expression in DAergic neurons was found to be cell-autonomous with Wt DAergic neurons from the RTT female and DAergic neurons from Wt females displaying similar amounts of α4* nAChRs on their soma. Finally, there was convincing evidence for spatially-modulated reduction in nAChR expression in mutant DAergic neurons with the lateral SNc showing a greater reduction in levels of nAChR expression compared to the medial SNc. To our knowledge, this is the first study to provide anatomical evidence for a cell-autonomous downregulation of α4* nAChR expression in DAergic neurons in the SNc of a young RTT female mouse.

Table of Contents

List of Figures

List of Tables

List of Abbreviations

AA	Amino acid
ACh	Acetylcholine
CNS	Central nervous system
cys	cysteine
DAergic	Dopaminergic
EC_{50}	Half maximal effective concentration
EGFP	Enhanced green fluorescent protein
GABA	γ-aminobutyric acid
LTD	Laterodorsal tegmental nucleus
MBD	Methyl binding domain
MeCP2	Methyl-CpG binding protein 2
MHb	Medial habenula
MT	Mutant
nAChR	Nicotinic acetylcholine receptor
PBS	Phosphate buffered saline
PFA	Paraformaldehyde
PFC	Prefrontal cortex
PPTN	Pedunculopontine nucleus
RN	Raphe nucleus
Rett Syndrome	RTT
ROI	Region of interest
SNc	Substantia nigra pars compacta
SNr	Substantia nigra pars reticulata
TH	Tyrosine hydroxylase
TRD	Transcription repressor domain
VTA	Ventral tegmental area
Wt	Wild-type
XCI	X-chromosome inactivation
YFP	Yellow fluorescent protein
*	Containing (*e.g.* α4* nAChR containing other receptor subtypes in addition to α4)

Acknowledgements

I would like to acknowledge the combined contributions of my two supervisors, Dr. Raad Nashmi and Dr. Kerry Delaney, to this research. Their knowledge, support, and advice were key to the successful completion of this project. In particular, I would like to individually thank Dr. Nashmi for his continued support when the mice kept us in the dark, and Dr. Delaney for teaching me not to trust anything but a warm cup of coffee. They have instilled the curiosity and work ethics necessary to see this study through. I would also like to acknowledge the great work of the mouse husbandry staff and the excellent technical support from Jay Leung. Huge thanks to Farnoosh Farhoomand and Azam Asgari for their continued help and camaraderie in the lab. Finally, I would like to thank members of the Awatramani and Chow labs for their support and friendship

Chapter 1 – Introduction

Recognized in the 1980s as a worldwide medical condition, Rett syndrome (RTT) is an X-linked progressive neurodevelopmental disorder resulting from *de novo* mutations in a gene encoding methyl-CpG binding protein 2 (MeCP2), a small transcriptional repressor (Rett, 1966; Hagberg et al., 1983; Amir et al., 1999). MeCP2 aberrations result in a constellation of severely debilitating symptoms including significant behavioral impairments which are hypothesized to be related to the loss of function of specific neuronal receptors such as the nicotinic acetylcholine receptor (nAChR), a member of the cys-loop receptor family (Wenk, 1997). Research on therapeutic approaches for RTT has shown that loss of MeCP2 functionality can be restored and in such cases many symptoms are dramatically reversed (Guy et al., 2007; Leung et al., 2017). However, due to potential genotype effects, treatments for RTT have to be designed with an understanding of the downstream effects of MeCP2 mutations on specific receptor families tailored to their involvement in different neuronal circuits. As such, examining the consequences of MeCP2 mutations on the expression and functionality of well-characterized receptors, such as nAChRs, is essential in order to identify the causes of the phenotypic characteristics seen in RTT and develop effective treatments.

1.1 Rett syndrome, An Overview

RTT is a postnatal progressive neurodevelopmental disorder with symptoms manifesting in stages during early childhood (Fig. 1).

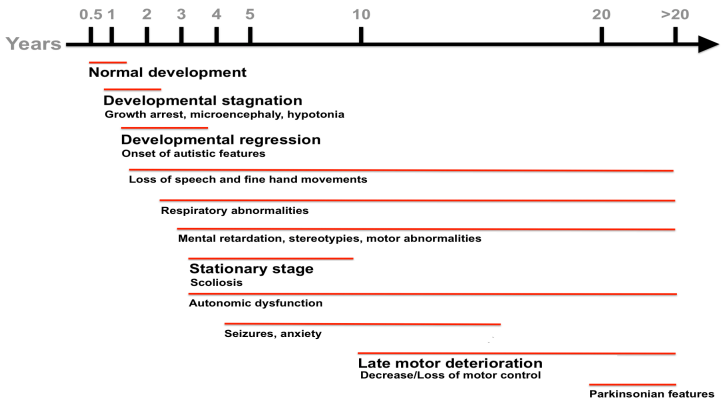

Figure 1. Onset and progression of clinical phenotypes in human RTT patients. After an initial normal development, babies enter a period of developmental stagnation followed by rapid neuronal regression resulting in severely impaired individuals. The condition stabilizes after twenty years and patients show lifespans similar to healthy humans. Modified from Chahrour and Zoighbi (2007).

Development is normal in the first 6-18 months but then stalls and regresses, resulting in individual that typically lack motor coordination, have impaired speech, and exhibit parkinsonian features later in life often accompanied by seizures (Hagberg, 2005; Jian et al., 2006; Roze et al., 2007). RTT has an incidence of ~1/8500 female live births (2017) and is almost always prenatally lethal in hemizygous males. Since more than 99% of the cases are due to *de novo* mutations in the paternal germline, it very hard to trace the disease except in extremely rare familial cases. Research examining a familial form of RTT identified mutations in the *MECP2* gene encoding X-linked methyl-CpG-binding protein 2 (MeCP2) as the primary cause of RTT (Amir et al., 1999).

1.1.1 Structure and Function of MeCP2

The *MECP2* gene located on the X chromosome is comprised of four exons that code for two different isoforms of the MeCP2 protein due to alternative splicing of exon 2 (Fig. 2).

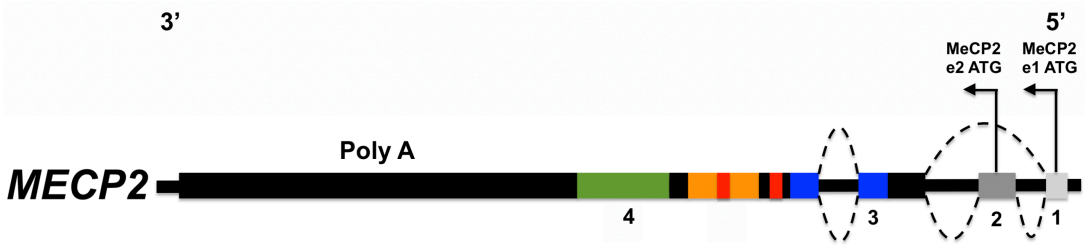

Figure 2. *MECP2* coding regions and functional protein domains. The four exons of the *MECP2* gene are numbered from 1 to 4 and shown in colour. In blue is represented the methyl binding domain (MBD), orange represents the transcription repression domain (TRD) and green shows the WW binding region. The two nuclear localization signals are displayed in red. Dashed line represents splicing events. Modified from Singh et al. (2008).

The splice variants differ only in the amino acid (AA) sequence at their N-termini with the MeCP2-e1 isoform containing the 24 AAs encoded by exon 1 and lacking the 9 AAs encoded by exon 2 while the start site for the MeCP2-e2 isoform is in exon 2 (Kriaucionis and Bird, 2004; Dragich et al., 2007). The full MeCP2 protein is 189 AAs long and although it is widely expressed in the human body, it is most abundant in the brain and specifically in mature neurons (Jung et al., 2003). While MeCP2 protein expression is low during embryogenesis, it increases progressively during the postnatal period of neuronal maturation (Miyake and Nagai, 2007). *MECP2* mutations do not result in defects in the proliferation and differentiation of neural progenitors, consistent with MeCP2 function restricted to mature neurons.

MeCP2 is a member of the methyl-CpG-binding protein family identified in mammals by Hendrich and Bird (1998) and consists of three domains: the methyl binding domain (MBD) that binds to methylated CpG islands of target genes, the transcription repressor domain (TRD), and a

C-terminal domain with the addition of two nuclear localization signals (Singh et al., 2008). The function of MeCP2 as a transcriptional repressor was first demonstrated in previous studies in which MeCP2 inhibited transcription from methylated promoters (Nan et al., 1997). It has since been found to be ubiquitously involved in gene repression, reporter splicing, transcriptional activation, and chromatin loop formation (Young et al., 2005; Nikitina et al., 2007; Zachariah and Rastegar, 2012). The large range of MeCP2 functions underlies the multifunctional character of the protein with clearly defined roles in chromatin remodelling and RNA splicing. As such, it is reasonable to envision that MeCP2 loss of function leads to a plurality of defects, many of which remain to be identified and characterized.

1.1.2 MeCP2 Loss of Function in Rett Syndrome

MECP2 mutations are found in more than 95% of RTT cases and typically involve cytosine to thymine base transitions at CpG dinucleotides (Wan et al., 1999; Trappe et al., 2001). Missense and nonsense mutations account for more than 70% of all reported gene mutations in RTT mouse models while C-term deletions and incorrect frameshift rearrangements accounting for 20% (Christodoulou et al., 2003; Ravn et al., 2005; Archer et al., 2006; Pan et al., 2006). C-term deletions and missense mutations tend to produce milder RTT phenotypes than early truncation or incorrect transcription of the nuclear localization signals (Smeets et al., 2005). Because mutations introduce premature stop codons that are predicted to result in a null allele, RTT is commonly associated with MeCP2 loss of function (Chahrour et al., 2008).

Of major interest is the phenotypic variability seen in RTT female patients. Following X chromosome inactivation (XCI), only one of the two alleles for *MECP2* is active in any given cell and the choice of which X chromosome is silenced is random. Therefore, females with RTT show cellular mosaicism with half the cells expressing the normal (wild-type, Wt) *MECP2* allele while the other half expresses the mutant (MT) *MECP2* allele. Since WT cells usually divide faster than MT cells in these patients, there is usually a shift in the distribution of XCI towards Wt cells that improves the RTT phenotype to sometime exhibit even an asymptomatic form of the disease; in the latter case, the disease is usually identified through the occurrence of RTT in the offspring of such patients, which show dramatic RTT symptomology (Dragich et al., 2000). Although rare, somatic mosaicism has also been reported as a source of phenotypic variability in RTT (Bourdon et al., 2001)

1.1.3 Mouse Models for Rett Syndrome

In the early 2000s, mouse models were created to study the structural and functional defects that underlie RTT (Chen et al., 2001; Guy et al., 2001). In this case, male knockouts for *Mecp2* survive postnatally but undergo severe developmental dysfunction around four weeks after birth leading to death around 8 to 10 weeks of age; female *Mecp2*$^{+/-}$ also show behavioral abnormalities but they develop at a later stage (around 3 months old) and while they are typically severely debilitated at six months, they can still survive to reproduce (Guy et al., 2001). Brains of *Mecp2* null mice are usually smaller in size compared to their WT littermates but they show no structural abnormalities nor increased neurodegeneration (Matarazzo et al., 2004). Not only do these mice display the same phenotypic characteristics seen in human RTT patients but experiments driving MeCP2 expression under the *tau* promoter showed rescue of the neurological phenotype of the mice, confirming Mecp2 loss of function as the main cause of the disease (Chen et al., 2001; Luikenhuis et al., 2004; Gemmelli et al., 2006).

Research on *Mecp2* knockout mice has revealed profound and systemic neurological dysfunction. First, electrophysiological experiments reported defects in long term potentiation and synaptic plasticity (Asaka et al., 2006; Moretti et al., 2006). Second, decrease in global synaptic activity was observed with a switch towards greater total synaptic inhibition (Dani et al., 2005; Nelson et al., 2006; Chao et al., 2007). Third, structural changes in dendritic and soma morphologies were also reported in pyramidal neurons, with a decrease in nuclear size (Rietveld et al., 2015). Finally, impaired modulatory role of MeCP2 in gene expression has been shown in several studies where defects in MeCP2 function led to dysregulation and non-functional expression of transcription factors, hormones, neuropeptides, and ionotropic receptors (Martinowich et al., 2003; Nuber et al., 2005; Samaco et al., 2005; McGill et al., 2006).

1.1.4 Reversibility of MeCP2 Dysfunction and Therapeutic Axes

The absence of premature neuronal cell death in RTT has sparked research to investigate whether restoring *MECP2* expression would rescue the neurological impairments exhibited by both patients and disease models. Previous studies by Guy et al. (2007) and Giacometti et al. (2004) showed that *cre*-mediated *Mecp2* expression in conditional knockout mice would cause sudden expression of *Mecp2* leading to either death or complete neurological rescue. Furthermore, it has been found that restoring the expression or function of downstream gene targets of Mecp2 would

lead to transient phenotypic restauration of neuronal functions in mouse knockouts. One such study by Leung et al. (2017) showed that acute injection of a pharmacological agonist targeting the nicotinic acetylcholine (ACh) receptor type would cause male mice to show fully restored locomotion for a short period of time. Therefore, it draws optimism for future treatments of RTT. However, with the multifunctional character of the MeCP2 protein and the phenotypic variability seen in RTT female patients, it is crucial to further identify and characterize neuronal circuits and specific receptor classes affected by MeCP2 loss of function in order to design effective treatments. One priority pertains to the basal ganglia loop and its modulation by ACh receptors as it plays a crucial role in the initiation and maintenance of all locomotor behaviors.

1.2 Basal Ganglia Motor loop: An Overview

In vertebrates, motor behaviors are initiated by excitatory inputs coming from regionalized populations of neurons in the central nervous system that synapse onto lower motor neurons in different segments of the spinal cord (Lundberg, 1975). These lower motor neurons in turn release acetylcholine at neuromuscular junctions to cause the muscle contractions necessary for body movements (Henneman, 1990). While the basal ganglia are not directly involved in the modulation of lower motor circuitry, they play a crucial role in the initiation and inhibition of motor behaviors by regulating of the activity of the upper motor neurons in the cerebral cortex (Kaji, 2001).

The term basal ganglia commonly refer to a set of distinct motor nuclei that are organized bilaterally within the cerebrum and midbrain: the striatum, which includes the caudate and the putamen, the external and internal segments of the globus pallidus, the subthalamic nucleus, and the thalamus (Fig. 3) (Gerfen and Wilson, 1996). During movement initiation, medium spiny neurons in the striatum are excited by transient excitatory inputs from the cerebral cortex which leads to transient inhibition of the tonically active inhibitory neurons in the internal segment of the globus pallidus, which project in turn to the subregions of the thalamus (Fig. 3) (Kocsis et al., 1977; Smith et al., 1998; Grillner et al., 2005). Inhibition of the globus pallidus results in transient disinhibition of tonically active neurons in the thalamus that provide excitatory inputs to the frontal cortex which ultimately excites upper motor neurons and initiates movement (Fig. 3) (Smith et al., 1998).

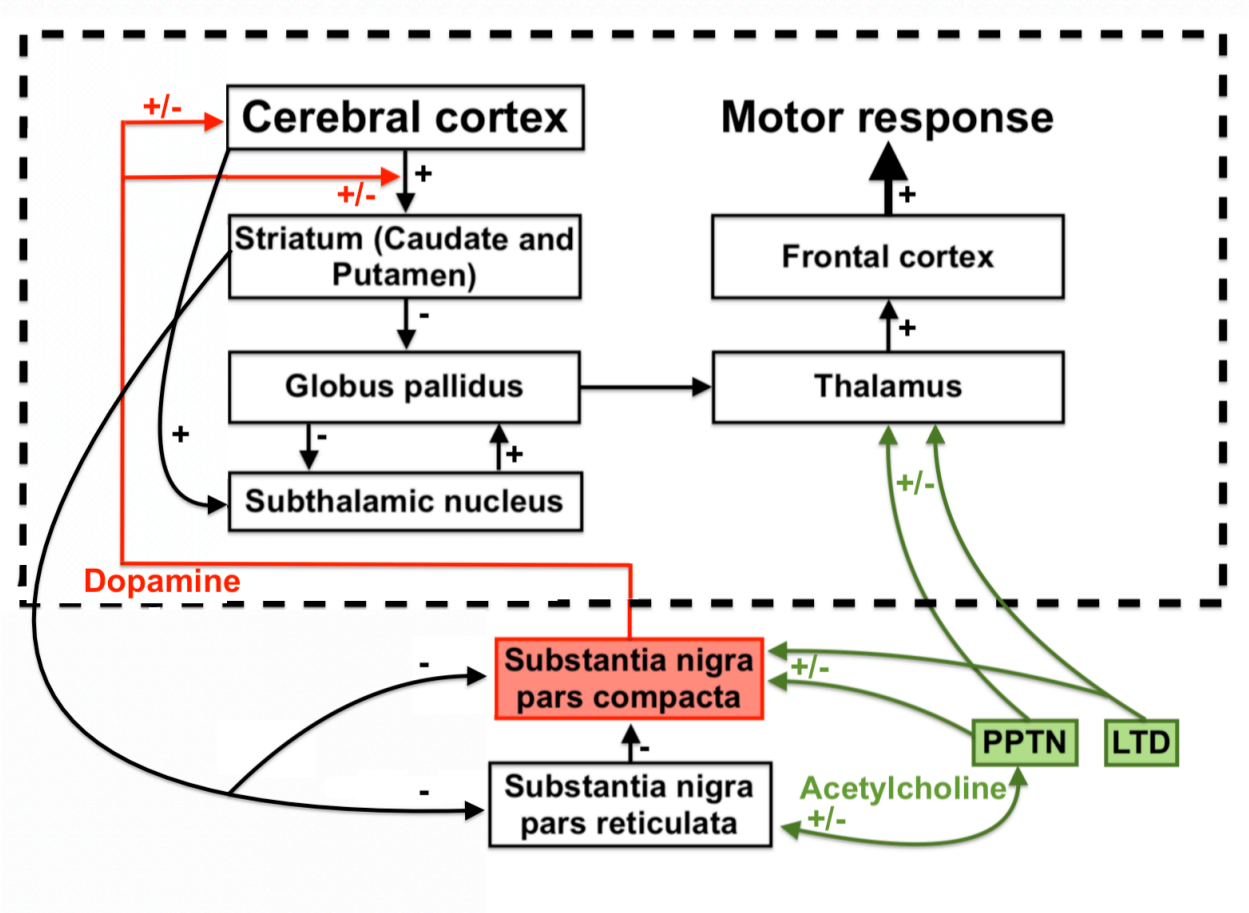

Figure 3. Functional organization of the circuitry of the Basal ganglia. The cerebral cortex sends excitatory inputs to the striatum that transiently inhibits the globus pallidus (GP), leading to disinhibition of thalamic nuclei that sends excitatory inputs to the frontal cortex that modulate upper motor neuron activity to initiate movement. Transient inactivation of the GP and inputs from the cerebral cortex leads to activation of the subthalamic nucleus that in turns excites the internal GP segment leading to thalamic inhibition and movement termination. The Nigrostriatal pathway exerts a crucial role in the integration of cortical inputs in the striatum: excitation of the substantia nigra pars compacta (in red) and pars reticulata by the striatum leads to differential activity of the cerebral cortex and the GP. The basal ganglia are also modulated by cholinergic projections from the pedunculopontine tegmental nucleus (PPTN, in green) and dorsolateral tegmental nucleus (LTD). Dopaminergic projections to the different nuclei or brain subregions are labelled in red, serotonergic projections in blue, and cholinergic projections in green. The dashed rectangle represents the cerebrum. Plus and minus arrows represent excitatory and inhibitory outputs, respectively. Modified from Purves (2018)

Movements are terminated by increase in the level of tonic inhibition mediated by the projection neurons of the internal segment of the globus pallidus (Smith et al., 1998; Purves, 2018). In this second pathway, a population of medium spiny neurons transiently inhibits tonically active inhibitory neurons in the external segment of the globus pallidus (Fig. 3). The external segment of the globus pallidus sends projections to the subthalamic nucleus which also receives excitatory projections from neurons in the cerebral cortex (Fig. 3). Disinhibition of the subthalamic nucleus and concurrent excitation from the cerebral cortex leads to an increase in excitatory activity of

subthalamic neurons that project diffusely back to the internal segment of the globus pallidus and the substantia nigra pars reticulata (SNr) (Fig. 3) (Purves, 2018).

An important circuit in the modulation of the basal ganglia system involves dopaminergic (DAergic) projections from the substantia nigra pars compacta (SNc) and is commonly referred to as the nigrostriatal pathway (Kemp and Powell, 1970; Tecuapetla et al., 2016). The pathway plays a crucial role in controlling the correct initiation, execution, and termination of movements, and was exemplified through studies examining neurodegenerative diseases where cellular defects in the SNc were found to cause profound behavioral impairments.

1.2.1 Influence of the Nigrostriatal Pathway on Movement

Although the nigrostriatal pathway only involves a small pool of DAergic neurons located in the SNc, it has great influence over the integration of cortical inputs in the striatum (Anden et al., 1966; Kemp and Powell, 1970; Nakamura and Hikosaka, 2006). The striatum projects to both the SNc and SNr with the former projecting back to the striatum while the latter provides delayed inhibition of those DAergic cells through GABAergic projections (Fig. 3) (Gerfen et al., 1990; Mink, 1996). The effects of the DAergic projections on the activity of medium spiny neurons in the striatum are complex and depend on the differential expression of two types of G-protein-coupled dopamine receptors in these neurons, D1 and D2 (Bateup et al., 2010). The difference between the two types of receptors is that the D1 type mediates the activation of G-proteins that increase the intracellular concentration of cAMP while the D2 type does the reverse (Purves, 2018). Differences in D1 or D2 DAergic receptor expression in spatially distinct striatal populations of medium spiny neurons lead to antagonistic effects in movement modulation by SNc neurons: DAergic projections to D1 receptor-expressing striatal neurons result in enhanced excitatory inputs and facilitates movement initiation while projections to D2 receptors negate this excitation (Yung and Shim, 2011; Purves, 2018).

Loss of this dopaminergic circuit may explain many basal ganglia disorder. A famous example relates to the premature loss of nigrostriatal DAergic neurons as the main cause of hypokinesia in Parkinson's disease: the destruction of DAergic cells contributes to an abnormally high inhibitory outflow of the basal ganglia that dramatically decreases the likelihood of movement initiation (Stegs and Johnels, 1994; Redgrave et al., 2010).

The excitability of both DAergic and GABAergic neuronal pools in the SN is also modulated by several other systems, which feed back onto the motor loop. One of them, the cholinergic system, has been found to be crucial in mediating the balance of excitation to inhibition (E/I) of the SN (Nashmi et al., 2007; Estakhr et al., 2017).

1.3 Structure and Expression of Acetylcholine Receptors in the Brain

In the mammalian nervous system, acetylcholine (ACh) receptors are divided into two main types: muscarinic ACh receptors, which are G-protein coupled receptors, and nicotinic ACh receptors (nAChRs), which are ligand-gated cation channels. nAChRs are further subdivided into the muscle nAChR subtype (composed of α, β, γ, δ and ε subunits) and the neuronal nAChR subtype (consisting of α2-α10, β2-β4 subunits) (Nashmi and Lester, 2006; Nashmi et al., 2007). While the muscle form of the nAChR is typically localized at the muscle and is involved in muscle contractions, neuronal nAChRs are found in PNS, CNS and other peripheral tissues (Whiting and Lindstrom, 1986; Whiting et al., 1987). α4β2 nACh receptor being the most prominent subtype in the brain (Whiting and Lindstrom, 1986).

nAChRs are members of the cys-loop family of pentameric ligand gated ion channels which are characterized by a disulfide bond near their extracellular N-terminus (Fig. 4). Each channel is thus formed by assembly of five subunits, which are denominated as either α, or β (Nashmi and Lester, 2006). While there are only single isoforms of γ and ε subunits, studies have identified nine different α subunits in vertebrates (α2-α10) and three β subunits (β2-β4) (Nashmi and Lester, 2006). While α7 subunits can form a fully functional homopentameric receptor, α2-α6 subunits must combine with β subunits to form functional pentameric receptors. Channel activation occurs following ligand binding at the junction between two α subunits or between an α and a β subunit, with the α subunit providing the double cysteine (cys-cys) residues that are required for ligand binding (Hansen et al., 2005).

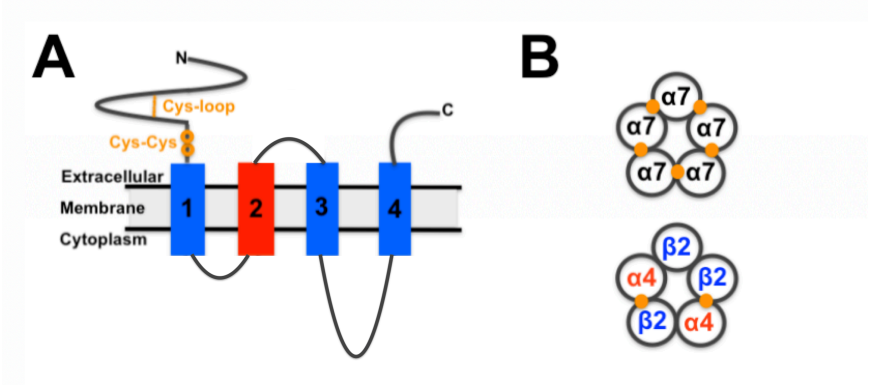

Figure 4. Structural representation of nAChR subunits and fully assembled receptors. A. Linear form of the subunit structure common to all α subunits. The cys-pair required for ligand binding is shown, as well as the highly conserved disulfide bridge near the N-terminus that is a hallmark to all members of the cys-loop family of ligand-gated ion channels. Only α subunits have the cys-pair in their AA sequence while all subunits possess the cys-loop. The 2nd transmembrane domain lining the pore of the channel is shown in red. **B**. Subunits combine to form pentameric receptors with five subunits lining a central pore. Subunits can either form homomeric receptors (as in the α7 nAChRs) or heteromeric receptors from combinations of α and β subunits. The ligand binding site are shown as orange dots at the junctions between subunits. Modified from Laviolette and Koy (2004).

ACh was first discovered by Otto Loewi and is the endogenous neurotransmitter for nACh receptors. ACh acts primarily as an excitatory neurotransmitter by depolarizing neurons postsynaptically or facilitating neurotransmitter release at the presynaptic terminal (Nashmi and Lester, 2006; McCoy and Tan, 2014). Upon acetylcholine binding, the nACh receptor channel opens and allows cation influxes of Na^+, Ca^{2+}, and K^+ that will cause membrane depolarization. Following ligand binding, the receptor only activates for a few milliseconds before degradation by acetylcholinesterase and reuptake by choline transporters.

Previous studies have shown that activation of nAChRs facilitates synaptic release of various neurotransmitters such as dopamine, GABA, glutamate, serotonin, ACh, and noradrenaline (Léna and Changeux, 1997; Gioanni et al., 1999; Cheer et al., 2007; Li and Eisenach, 2002; Araque et al., 2002; Kenny et al., 2000; Estakhr et al., 2017). Other research also found that nAChRs localized on neuronal cell bodies and axon terminals mediate synaptic transmission by generating EPSPs and increasing neuronal excitability (Roerig et al., 1997; Albuquerque et al., 2000; Léna et al., 1993).

Nicotinic receptor expression is variable throughout the brain and there are several nicotinic receptor subtypes with different dynamics. The most prominent nAChR subtype in the brain, α4β2 (Whiting and Lindstrom, 1986), plays a crucial role in ACh-mediated behavior and is predominantly expressed in both DAergic and GABAergic neuron pools in the substantia nigra.

1.4 Functional Characteristics of α4β2 nAChR

α4β2 nAChRs are high affinity receptors that are expressed in a large proportion throughout regions of the mammalian brain (Whiting and Lindstrom, 1986). In particular, studies have reported the presence of α4β2 nAChRs in the cell bodies of cholinergic neurons of the medial habenula, the medial perforant path of the hippocampus, and DAergic and GABAergic neurons of the SN and VTA (Nashmi et al., 2007; Renda and Nashmi, 2012, 2014; Renda et al., 2016). α4β2 nAChR expression at these key regions mediate widespread behaviors that are essential to normal mammalian function.

1.4.1 Subunit Stoichiometry of α4β2 nAChR

Upon subunit assembly, α4β2 nAChR can adopt either one of two different stoichiometries: $(\alpha4)_3(\beta2)_2$ or $(\alpha4)_2(\beta2)_3$. A difference in receptor stoichiometry will affect its sensitivity to ACh and nicotine, its exogenous ligand. Indeed, studies have shown that while the $(\alpha4)_2(\beta2)_3$ conformation has a high ligand affinity with an EC_{50} equal to 1.6 μM for ACh, the more common $(\alpha4)_3(\beta2)_2$ (~82%) has a much lower affinity for ACh with an EC_{50} of 62 μM (Buisson and Bertrand, 2001; Nelson et al., 2003). In the brain, the situation is more complex in that other subunits can also combine with α4 and β2 to form a rich repertoire of cholinergic signalling.

1.4.2 Cholinergic Modulation of the Nigrostriatal Pathway and its Possible Defects in RTT

DAergic neurons in the SNc have one of the highest expression of nAChRs in the brain (Nashmi et al., 2007). Two brainstem nuclei provide the majority of cholinergic inputs to the SNc: the pedunculopontine nucleus (PPTN) and the laterodorsal tegmental nucleus (LTD (Fig. 3) (Clarke et al., 1987; Cornwall et al., 1990). SNc DAergic neurons are strongly excited by nicotine, however, the extent to which the LTD and the PPTN modulate DAergic activity in the SNc still remains unclear (Nashmi et al., 2007). A recent study by Estakhr et al. (2017) reported heterogeneous responses to evoked ACh release in the SNc with activation of cholinergic terminal projections in the medial SNc decreasing locomotion whereas activation in the lateral SNc increased locomotion. The study's result was in line with previous research that reported that while the overall PPTN activity positively correlated with the initiation of motor responses, the activity of subpopulation of PPTN neurons negatively correlated to movement (Matsumura et al., 1997; Norton et al., 2011).

This paradoxical effect of cholinergic inputs onto the SNc underlies a paradox in the modulation of motor behavior by the cholinergic system, which, if impaired, might explain some of the phenotypic characteristics seen in RTT patients and disease models. Indeed, research examining differences in locomotor responses in a RTT mouse model following acute injections of an α4β2 nAChR agonist reported a strong reversal in locomotor suppressive characteristics following agonist injections in RTT mice compared to their WT littermates as well as overall downregulation of α4β2 nAChR mRNA in these mutant mice (Leung et al., 2017). However, there were differences in motor response between male and female RTT mice following the exogenous activation of nAChRs by either nicotine or TC-2559, both strong nAChR agonists with TC-2559 being specific to α4/α6 nicotinic receptors (Leung et al., 2017). As such, differences in the expression and the extent of the functionality of α4β2 nAChR in SNc DAergic is still yet to be examined.

1.5 Research Objective and Hypothesis

1.5.1 Research Objective

Our objective is to develop an experimental model of α4-containing (α4*) nAChR imaging in RTT female mice that permits us to quantify with great spatial resolution the expression of α4 nAChR protein between MT and Wt cells at key brain regions involved in the modulation of locomotor behaviors. Attempting to quantify receptor expression using laser confocal microscopy is a difficult task that requires the testing and control of many variables before applying the techniques to examine potential cellular defects in a RTT mouse model. By crossbreeding three different mouse strains, we hope to be able to create a robust, accurate, and replicable assay that will ultimately allow us to implicate downregulation of α4* nAChRs as one of the causes for the severe motor defects seen in RTT patients.

1.5.2 Hypothesis

We will test the hypothesis that, in the SNc of a RTT female mouse, mutant DAergic cells have downregulated α4* nAChR expression compared to Wt DAergic cells. We also hypothesize that this effect is cell autonomous, i.e. the Wt DAergic cells in RTT female mice will have similar levels of α4* nAChR expression compared to that of their Wt littermates.

Chapter 2 – Materials and Methods

2.1 Animal care and breeding

All experiments were conducted in accordance with the guidelines for the care and use of animals set by the Canadian Council on Animal Care (CCAC). Mice were housed at the University of Victoria Animal Care Unit (UVic ACC) and all protocols were approved by the University of Victoria Animal Care Committee. Mouse strains used in this study included *Mecp2*$^{EGFP/+}$, *α4*$^{YFP/+}$ (Nashmi et al., 2007), and *Mecp2*$^{+/-}$ (*Mecp2*$^{tm1.1Jae}$ /Mmcd (MMRRC, UC Davis) (Chen et al., 2001). Mice were kept on a standard 12 hour light:dark cycle and given food and water *ad libitum*. The α4-YFP knock-in mouse strain has a single mutation in which a gene sequence coding for a yellow fluorescent protein (YFP) has been inserted in the M3 to M4 loop of the α4nAChR subunit. α4* nicotinic receptor subtypes have been shown to express and function normally in comparison to their wildtype littermates (Nashmi et al., 2007). The *Mecp2*$^{+/-}$ mouse strain has an in-frame N-terminal deletion of *Mecp2* exon 3 (Chen et al., 2001). The *Mecp2*$^{EGFP/+}$ knock-in mouse strain has an EGFP sequence inserted in the 3'UTR region of the *Mecp2* gene (Chahrour et al., 2008). *Mecp2*$^{EGFP/+}$ females were crossed with homozygous α4-YFP knock-in males to generate *Mecp2*$^{EGFP/+}$/ *α4*$^{YFP/+}$ offspring. A similar cross-breeding strategy was used between *Mecp2*$^{+/-}$ females and homozygous α4-YFP knock-in males to generate offspring heterozygous for both *Mecp2* and *α4*. Five-week-old (P35) female offspring from these two new mouse strains were used for the α4-YFP quantification experiments. Mice were weaned at 20 days old and divided by sex into groups of 2-5 littermates at 30 days. Two separate sets of PCRs were performed to confirm both *α4* and *Mecp2* statuses (Nashmi et al., 2007; Stuss et al., 2012).

2.2 Intracardial perfusion and brain slice preparation

Following fifteen days of weaning, mice were sacrificed, and their brain harvested for quantitative fluorescence imaging of *α4YFP* in the medial habenula and the substantia nigra pars compacta.

Mice were anaesthetized via an inhalant form of isoflurane. Once unresponsive, the animal was pinned down ventral side up and a longitudinal incision in the stomach was made to open the abdomen. Two other incisions were made parallel to the sternum on each side of the ribcage and the diaphragm was sectioned horizontally. Ribs were then removed using a bilateral oval cut to

expose to the heart. A 23 G butterfly needle (Becton Dickinson, cat#367253) was inserted into the left ventricle while the right atrium was cut to provide an exit for deoxygenated blood and perfusate. Solutions were then pumped at a rate of 4 mL/min by a peristaltic pump (Masterflex Easy Load, Cole-Parmer, cat#EW-07518-00). All solutions were prepared one day prior to the intracardial perfusion and left at 4°C overnight. The perfusion began with 25 mL of PBS (pH 7.6), followed by 25 mL of % paraformaldehyde (pH 7.6, diluted with 1X PBS from a 16% PFA stock; Electron Microscopy Sciences, cat#15710), and 5% sucrose (pH 7.6, mixed with 1X PBS from powder; EMD chemicals, cat# SX1075-3) in order to flush residual PFA and to reduce autofluorescence of the tissue. At the end of the perfusion, the mouse was decapitated, and the brain was extracted from the skull and put into a 30% sucrose solution (pH 7.6, mixed with 1X PBS). After two days in the dark and kept at a constant temperature of 4°C, the brain was removed from solution and a razor blade was used to remove the cerebellum. The brain was then placed rostral side up in a plastic embedding mold (VWR international, cat#18986-1), submerged in O.C.T Mounting medium (Tissue-Tek, cat#4583) and frozen in dry ice for 15 min before slicing. 30 µm thick coronal sections were cut using a cryostat (Leica CM1860UV) and put on poly-L-lysine-coated slides (NewSilane, Newcomer Supply, cat# 5070, or Superfrost® Plus Gold, Fisher Scientific, cat# 15-188-48) which were kept in slide boxes containing a calcium sulphate stone to mitigate freezer burn. Boxes were consequently stored in zip-lock plastic bags at -20°C.

2.3 Immunohistochemistry

Brain sections on slides were washed three times with 1X PBS (pH 7.6) for 10 min and then permeabilized with 0.25% Triton X100 for 10 min. The sections were washed again three times for 10 min with 1X PBS and successively blocked with 10% donkey serum (diluted in 1X PBS from stock; Jackson ImmunoResearch, cat# 017-000-121) for 30 min. The primary antibody (tyrosine hydroxylase polyclonal antibody, Pel-Freez, cat# P4010-0; MeCP2 polyclonal antibody, Millopore, cat# ABE171) was diluted in 3% donkey serum (diluted in 1X PBS) at 1:250 and incubated at room temperature overnight. Sections were washed with 1X PBS three times for 10 min. The secondary antibody (Alexa Fluor 405 IgG secondary antibody, Invitrogen, cat# A-31556; Cy3 IgG secondary antibody, Jackson ImmunoResearch Labs, cat# 711-165-152) was diluted in 3% donkey serum, at 1:500 concentration and incubated overnight at room temperature. Brain sections were then washed with 1X PBS three times for 10 min. For the imaging of the medial

habenula, NeuroTrace 435/455 (Invitrogen, cat# N21479) was applied to the slices at 1:200 concentration (mixed with 1X PBS) for one hour. Finally, sections were washed three times for 3 hours and mounted with 40 µL Immunomount (Immu-MountTM, Thermo Scientific, cat# 9990402). Following coverslipping, slides were left at 4°C overnight before imaging.

2.4 Spectral Confocal Imaging

Images were collected using spectral confocal microscopy. In order to accurately quantify the α4YFP fluorescence, great care was taken to ensure that sections were exposed to equal and minimal amounts of light before imaging. As such, the photobleaching of the fluorophore was kept low throughout the experimental procedure. Images were acquired using a Nikon C1si spectral confocal microscope. Sections were imaged with a 60X oil-immersed Plan Apo VC objective (1.4 NA, 0.13 mm working distance) and YFP was excited using a 514 nm laser line at 8% maximum emission of a 40 mW Argon laser. Images were collected at 5.52 µs pixel dwell time and averaged over 4 scans through a 60 µm dimeter pinhole with a spectral detector gain set at 220. Settings were optimized to ensure that greyscale intensity values fell below saturating value (<4095 for 12-bit greyscale) and kept consistent across all images and experiments. I collected 212x212 μm^2 z-stack images with a 1 µm step size over a 10 µm depth across a spectral range of 479.8-559.5 nm. The imaging software creates a λ-stack image; each pixel in the 512x512 $pixel^2$ XY image is made up of a complete spectral emission profile over 80 nm, at 2.5 nm resolution. I used a linear unmixing algorithm to deconvolve specific YFP fluorescence from GFP fluorescence, background autofluorescence, and CY3-specific fluorescence. We first obtained both GFP and YFP reference spectra by imaging HEK293T cells transfected with soluble YFP and GFP markers. We created a reference spectrum library by imaging brain regions of interest in one WT C57BL6J five-week-old female. By imaging this wildtype mouse as if I was measuring somatic YFP expression, the residual background level of autofluorescence on each cell type in each brain region was also obtained and subtracted from the final YFP intensity values to account for autofluorescence that has a similar signature to YFP and therefore cannot by removed by spectral unmixing. Once separated, autofluorescence was discarded and the remaining image displayed gray values only pertaining to specific YFP expression.

2.5 Analysis of Cell Body/Region-specific Expression of α4YFP and cell size.

Slices were labelled with NeuroTrace 435/455 (medial habenula) or tyrosine hydroxylase/Cy3 (substantia nigra pars compacta (SNc)) and MeCP2/Alexa Fluor 405, and analyzed using ImageJ software (Version 1.51m9, National Insitutes of Health, USA; https://imagej.nih.gov/ij). Regions of interest (ROIs) were drawn differently depending on the brain region. For coronal slices of the medial habenula and medial perforant pathway, one 212x212 μm-wide region was imaged for each hemisphere and a ROI was drawn around the area either defined by the three most lateral columns of neural cells (medial habenula) or encompassing the ventral two thirds of the tract (medial perforant pathway) and averaged over a summed intensity projection of the five optical slices with the highest mean overall intensity. For coronal slices of the SNc (Fig. 5), three 212x212 μm regions were imaged for each hemisphere: the first region was located medial to the oculomotor nerve and focused on the medial SNc while the two other regions were focused on the lateral SNc.

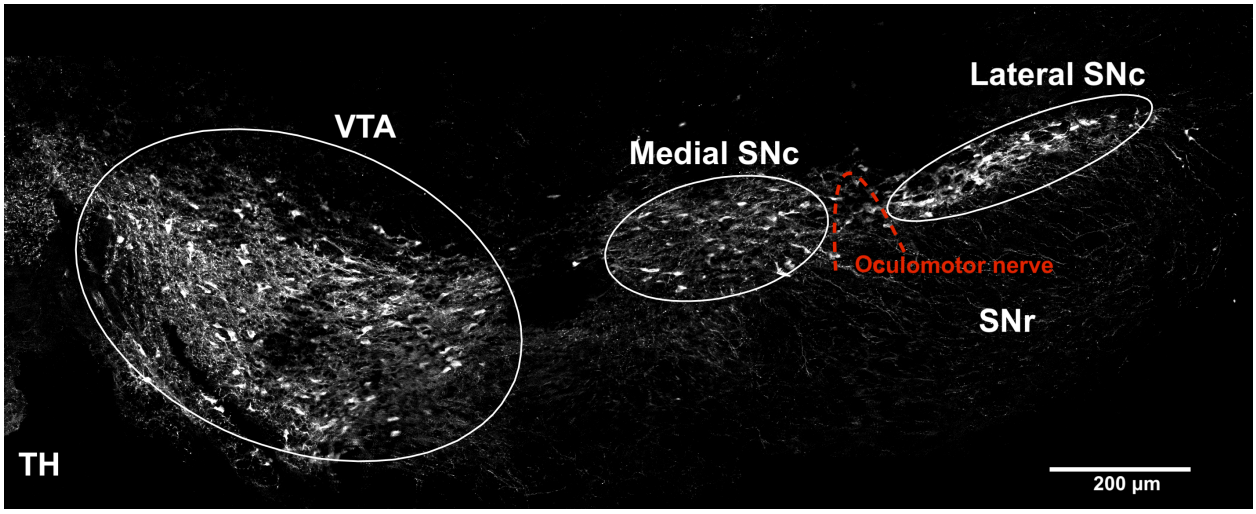

Figure 5. Immunohistochemical labeling of tyrosine hydroxylase shows spatially distinct DAergic neuron populations for the ventral tegmental area and the lateral and medial portions of the substantia nigra pars compacta. Low magnification z-projection (sum) of five optical slices from the right hemisphere of a P35 *Mecp2*$^{+/+}$/*α4*$^{YFP/+}$ female mouse. TH immunolabeling shows strong tyrosine hydroxylase expression in the VTA and SNc. The medial and lateral portion of the SNc are well defined and separated by the oculomotor nerve (in red) (Franklin and Paxinos, 1997). Dendritic projections of SNc DAergic neurons into the SNr are visible. Endogenous α4-YFP expression was examined in DAergic neuron populations from both lateral and medial portions of the SNc.

TH-positive cells in the SNc were analyzed on a cell-by-cell basis; for each cell, a ROI was drawn around the soma and a surface plot was used to find the optical slice showing the middle of the cell across the z-plane. A z-projection of five optical slices including two slices above and two slices below the optical slice labelling the middle of the soma was then computed and a final ROI was drawn around the cell body and used for quantification. A small ROI was taken from the z-projection during the measurement in a tissue region devoid of cell bodies to account for the residual background fluorescence in the YFP channel itself.

2.6 Statistical Analysis

Values are reported as mean ± standard error of the mean (S.E.M) and were computed using R (v3.4.1, 2014; https://www.r-project.org). Data were graphed using Igor Pro software. When applicable, assumptions of normality and equal variances were tested using a Shapiro-Wilk normality test and a *F*-test, respectively. Wilcoxon rank-sum tests were used to evaluate differences in mean when parametric assumptions were not met. If both parametric assumptions were satisfied, either a two-sample Student's t-test or a one-way analysis of variance (ANOVA) was used to evaluate the data; if both samples had normal distribution but unequal variances, a Welch's t-test was used to examine differences between the two means. Statistical significance was determined at the alpha level of .05 in all analyses.

Chapter 3 – MeCP2 Tagged with EGFP Does Not Affect Cell Size and α4 nAChR Subunit Expression in DAergic SNc Neurons of Five-week-old Female Mice

3.1 Introduction

As described in 1.4.2, dopaminergic neurons in the SNc have high expression of nicotinic receptors with the α4β2 subtype being the most predominant (Whiting and Lindstrom, 1986; Nashmi et al., 2007). SNc DAergic neurons are strongly excited by nicotine and their activation has been shown to modulate differential locomotor responses in mice (Nashmi et al., 2007; Estakhr et al., 2017; Leung et al., 2017). By placing the yellow fluorescent protein under the control of the native α4 promoter, we can quantify the α4-YFP fluorescence as an indirect measurement of α4ß2 nAChR expression. Using heterozygous $\alpha4^{YFP}$ offspring from a cross with a well-characterized knock-in mouse line containing a fluorescently labelled α4 nicotinic receptor, we can image the intensity of the α4-YFP signal with high spatial accuracy While the quantification of absolute fluorescence levels at a cellular scale may vary depending on the genotype of the animal, the brain region being imaged, and the experimental approach of the study, it is a perfectly valid and reliable tool when it comes to evaluate differences in fluorescence levels between two neuronal cell populations that are colocalized and share identical functional characteristics. Such cell populations can be created within the same brain region, e.g. the SNc, using targeted mutations and endogenous sex chromosome silencing (X-inactivation) in female mice.

Insertion of an EGFP sequence in the 3'UTR region of the *Mecp2* gene allows for accurate imaging of endogenous MeCP2 expression in the mouse brain (Chahrour et al., 2008). Homozygous male and female mouse carriers for the mutation are known to be viable, fertile, normal in size, have no behavioral or physical abnormalities, and have levels of MeCP2 expression that are similar to that of wildtype mice (Chahrour et al., 2008). Since *Mecp2* mutations are linked to Rett syndrome, this mouse strain is a useful model for visualizing MeCP2-expressing neuronal cells. Female offspring from our first crossbreeding strategy are heterozygous for both $Mecp2^{EGFP}$ and $\alpha4^{YFP}$; while the heterozygous trait leads to a reduction in total YFP fluorescence for the α4 mutation, it also results in two distinct neuronal cell populations in female mice for $Mecp2^{EGFP}$ due to X-inactivation (half of the cells will have the GFP signal while the other half will not). However, those two cell populations are otherwise genotypically identical and,

Based on the phenotype of the carriers homozygous for the mutation, are expected to show similar levels of α4ß2 nAChR expression in DAergic SNc neurons.

YFP and EGFP share overlapping excitation and emission spectra: the excitation and emission peaks for EGFP are 488 and 509 while that of YFP are 514 and 527 (Thastrup et al., 2001; Nagai et al., 2002). The great overlap in fluorescence signal between the two fluorophores makes them impossible to spatially separate when colocalized using standard confocal microscopy. However, with a highly technical imaging approach involving spectral confocal laser microscopy, one can try to resolve the fluorescence signal crossover to spectrally unmix the two spatially colocalized fluorophores.

Spectral confocal microscopy combines both the fields of spectroscopy and microscopy in order to be able to determine both the intensity and spectral properties of a specimen for each pixel in an image (Zimmermann, 2005; Larson, 2006; Nashmi, 2016). In order to measure the spectrum of an absorbing fluorophore, the emitted light is dispersed into its component wavelengths and the intensity for narrow bands of wavelength is measured (Larson, 2006). The measured signal across each component wavelength for each pixel of the field of interest is integrated in a three-dimensional dataset known as a lambda stack (Larson, 2006; Nashmi, 2016). The lambda stack represents an image collection using the same field acquired at different wavelength bands, each spanning a limited spectral region ranging from 2.5 to 10 nanometers (Larson, 2006). The analysis of these spectral images involves mathematical algorithms and is commonly referred to as linear unmixing (Zimmermann, 2005; Larson, 2006; Nashmi, 2016). The original purpose of hyperspectral imaging and linear unmixing algorithms was to determine the different types of terrains on the planet's landscape imaged by remote sensing satellites but the principles of this technique were subsequently applied to laser confocal microscopy to detect and separate fluorescence from a number of fluorescent molecules with overlapping emission spectra within a tissue sample. Linear unmixing algorithms are based on the assumption that the emission signal from a specimen is linearly proportional to the sum of the concentrations of the emission spectrum of each individual fluorophore making up the specimen (Zimmermann, 2005; Nashmi, 2016). The concept of unmixing is as follows: each pixel in an image is categorized as representing a mixture of fluorophore intensities (Zimmermann, 2005). The measured spectrum ($I(\lambda)$) can be deconvolved into the concentration (C) of each individual fluorophore reference spectrum ($R(\lambda)$) when the values are summed. Each reference spectrum of a pure fluorophore is described as $R_i(\lambda)$ where i represents the index of fluorophores in the specimen from i = 1, 2, 3...n. For n fluorophores, the relationship can be modelled as:

$$I(\lambda) = C_1R_1(\lambda) + C_2R_2(\lambda) + C_3R_3(\lambda) + \ldots\ldots + C_nR_n(\lambda), \text{ or } I(\lambda) = \sum_i C_iR_i(\lambda)$$

In practice, the intensity (I) for each pixel in the image is determined during acquisition of the lambda stack and the reference spectra were obtained from the imaging of pure fluorophores under specific laser settings (Zimmermann, 2005; Larson, 2006; Nashmi, 2016). The spectral contributions of each fluorophore can then be determined using a simple linear algebra matrix and the solution is obtained through an inverse least fitting square equation that minimizes the square difference between the measured and calculated spectra (Zimmermann, 2005; Larson, 2006; Nashmi, 2016). Considering its inherent advantages and its suitability with regards to my experimental approach, I used spectral confocal microscopy to investigate whether I can resolve spatially and spectrally overlapping EGFP and YFP signals in SNc DAergic cells of five-week-old female mice.

3.2 Results

3.2.1 The Mouse Medial Habenula and Medial Perforant Pathway Are Used as α4 nAChR Expression Controls*

The medial habenula (MHb) and the medial perforant pathway of the hippocampus were used as controls for α4-YFP fluorescence (Fig. 6A; 6B; 6C). I replicated the results of previous studies (Nashmi et al., 2007; Renda and Nashmi, 2012) with regional expression of α4 nAChR subunits being greater in the medial habenula compared to the medial perforant path ($p = 0.029$, $W = 16$, Wilcoxon rank-sum test) (Fig. 6D).

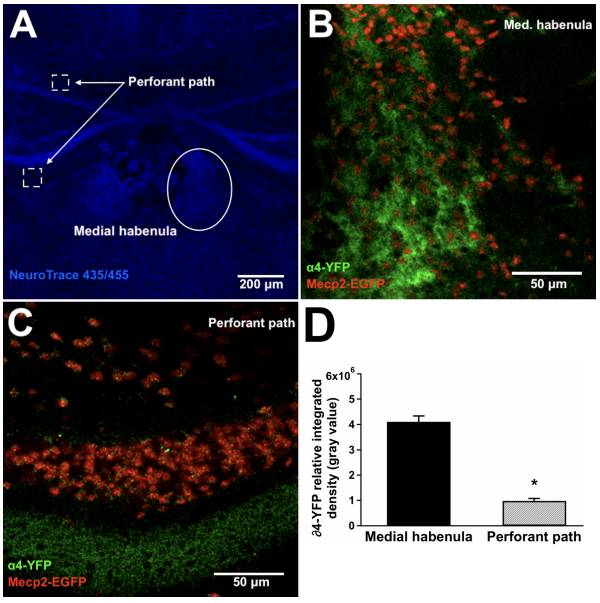

Figure 6. The medial habenula and the medial perforant path are used as α4* nAChR expression controls. A. Low magnification image showing a coronal view of the medial habenula (MHb) lining the third ventricle and the perforant path above and below the pyramidal blades of granule cell layers composing the dentate gyrus of a P35 $Mecp2^{EGFP/+}/\alpha4^{YFP/+}$ female mouse. Neuronal cell bodies were labelled with NeuroTrace to identify and target regions of interest. **B**. Endogenous α4-YFP expression on cholinergic MHb neurons. Note the medial to lateral increase in α4* nAChR expression. **C**. Endogenous α4-YFP expression on glutamatergic fibers found in the medial perforant path. **D**. α4 nAChR subunit expression, measured as relative integrated fluorescence density (arbitrary units), is much greater in the MHb compared to the medial perforant path ($p = 0.029$, $W = 16$, Wilcoxon rank-sum test), as predicted from previous studies. Each region was imaged once in both hemispheres for P35 $Mecp2^{EGFP/+}/\alpha4^{YFP/+}$ mice (n =4).

3.2.2 MeCP2 Tagged with EGFP Does Not Affect Cell Size and α4 nAChR Subunit Expression in DAergic SNc Neurons

I examined the effects of the MeCP2-EGFP mutation on soma size and α4* nAChR expression levels in P35 female mice heterozygous for *MeCP2*^{EGFP} and *α4*^{YFP}. I assessed if differences in soma size and α4YFP fluorescence densities could be detected between EGFP-positive (*MeCP2*$^{EGFP+}$) and EGFP-negative (*MeCP2*$^{EGFP-}$) DAergic cells in the SNc (Fig. 7A-F; Fig. 8; Appx.).

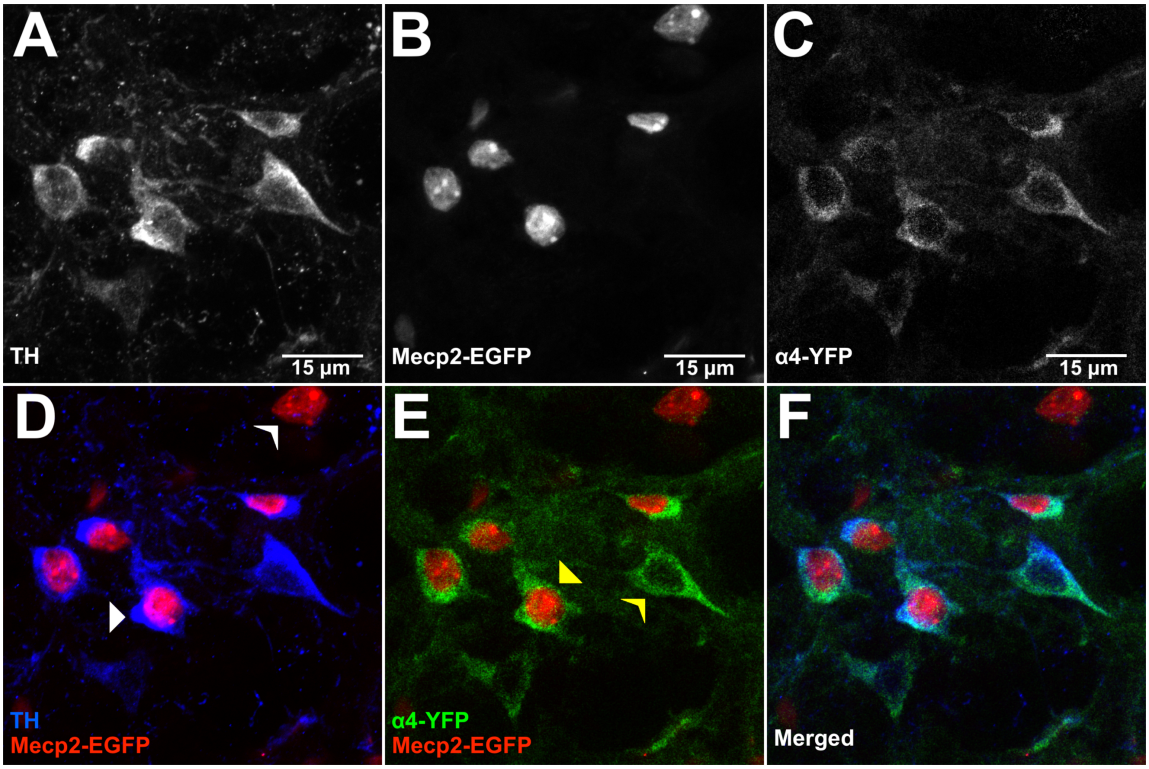

Figure 7. Endogenous expression of MeCP2-EGFP shows colocalized EGFP^{+} and EGFP^{-} DAergic SNc neurons as a consequence of random X chromosome silencing in *Mecp2*$^{EGFP/+}$/*α4*$^{YFP/+}$ female mice. A-F. Immunohistochemical labeling of DAergic (TH, **A**) neurons of the SNc showing endogenous MeCP2-EGFP (**B**) and α4-YFP (**C**) expression. **D**. Composite overlap showing specific TH labeling of DAergic neurons. Full white arrow shows a DAergic (TH-positive) cell. Slant white arrow shows a TH-negative cell. **E**. Composite overlap showing α4-YFP expression on MeCP2-EGFP^{+} and MeCP2-EGFP^{-} DAergic neurons. Full yellow arrow shows MeCP2-EGFP^{+} cell. Slant yellow arrow shows MeCP2-EGFP^{-} cell. **F**. Composite overlap showing differences in spatial expression of α4-YFP on DAergic neurons of the mouse SNc.

TH labeling showed no difference in cell size between GFP positive and GFP negative DAergic neurons ($p = 0.38$, $t = 0.89$, $df = 100$, two sample t-test) (Fig. 8A). Both GFP positive and GFP negative DAergic neurons also showed similar levels of α4YFP nAChR subunit expression ($p = 0.28$, $t = 1.09$, $df = 100$, two sample t-test) (Fig. 8B). Results concurred with previous studies investigating the physical and behavioral characteristics of MeCP2-EGFP knock-in mice and the levels of α4* nAChR expression in α4-YFP knock-ins, which added strength to the reliability of the experimental approach and the accuracy of the spectral unmixing between EGFP and YFP (Chahrour et al., 2008; Renda and Nashmi, 2012, 2014).

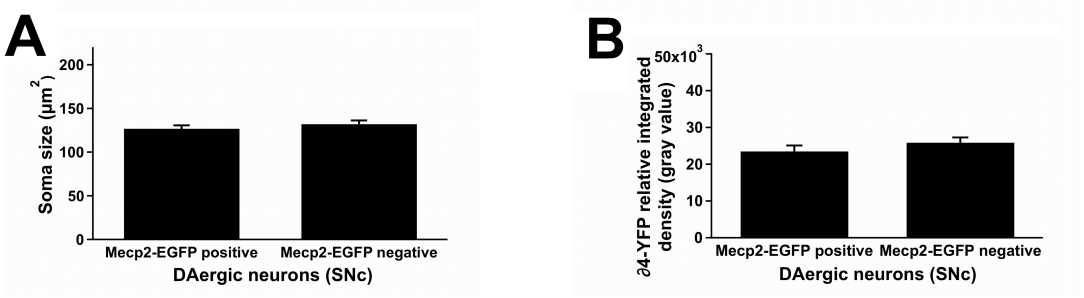

Figure 8. MeCP2 tagged with EGFP does not affect cell size and α4* nAChR expression in DAergic SNc neurons of P35 *Mecp2*$^{EGFP/+}$/*α4*$^{YFP/+}$ female mice. **A**. TH labeling of the cell bodies of DAergic neurons of the SNc shows no statistical difference in soma size between MeCP2-EGFP-negative (n=48) and MeCP2-EGFP-positive (n=54) cells ($p = 0.38$, $t = 0.89$, $df = 100$, two sample t-test). **B**. The EGFP sequence inserted in the 3'UTR region of *Mecp2* also does not affect α4 nAChR subunit expression in these DAergic neurons ($p = 0.28$, $t = 1.09$, $df = 100$, two sample t-test). All n values expressed as a number of cells taken from P35 *Mecp2*$^{EGFP/+}$/*α4*$^{YFP/+}$ mice (n =2)

Chapter 4 – Five-week-old Rett female mouse shows a cell-autonomous reduction of α4* nAChR expression levels in DAergic neurons of the SNc

4.1 Introduction

Mice are a useful model for studying the consequences of MeCP2 loss-of-function at a cellular level. Research of *Mecp2* knockout mice has already revealed important defects in neurological systems. The identification of such defects helps develop therapeutic strategies to alleviate or control the symptoms associated with Rett syndrome. However, due to the multifunctional properties of MeCP2 and the phenotypic variability associated with RTT female patients, there are still many circuits and transmitter systems to remain to be characterized as being altered or not by MeCP2 dysfunction. The modulation of DAergic neuron activity of the substantia nigra by the cholinergic system is of particular importance in this study with regards to its involvement in the generation and inhibition of motor responses. Furthermore, a recent behavioral study has found results that may indicate a dysregulation in the expression of α4* nAChRs in the mouse brain but research evaluating of α4 nAChR subunit expression in distinct neuron populations in a RTT mouse model has yet to provide anatomical correlates to this study (Leung et al., 2017). Since Rett female mice show cellular mosaicism with half the cells expressing the normal *Mecp2* allele while the other half expresses the mutant *Mecp2* allele, my goal is to quantify levels of α4* nAChR expression in both mutant and wildtype (Wt) dopaminergic neurons in the substantia pars compacta of a five-week-old Rett α4-YFP female mouse. With this female RTT mouse model and the same experimental approach that was used for the $Mecp2^{EGFP/+}/\alpha4^{YFP/+}$ mice, I hope to implicate α4ß2 nAChR downregulation as a consequence of MeCP2 loss-of-function in DAergic SNc neurons.

4.2 Results

4.2.1 Mutant SNc DAergic Neurons Have a Cell-autonomous Reduction in α4 nAChR Expression in a Five-week-old Rett α4-YFP Female Mouse*

Following the immunohistochemical labeling of MeCP2 and tyrosine hydroxylase (TH) and the imaging of coronal sections of the entire SNc for both wildtype and Rett female brains, I examined the effects of MeCP2 loss-of-function on soma size and α4 nAChR subunit expression in dopaminergic neurons (Fig. 8, 9; Appx.).

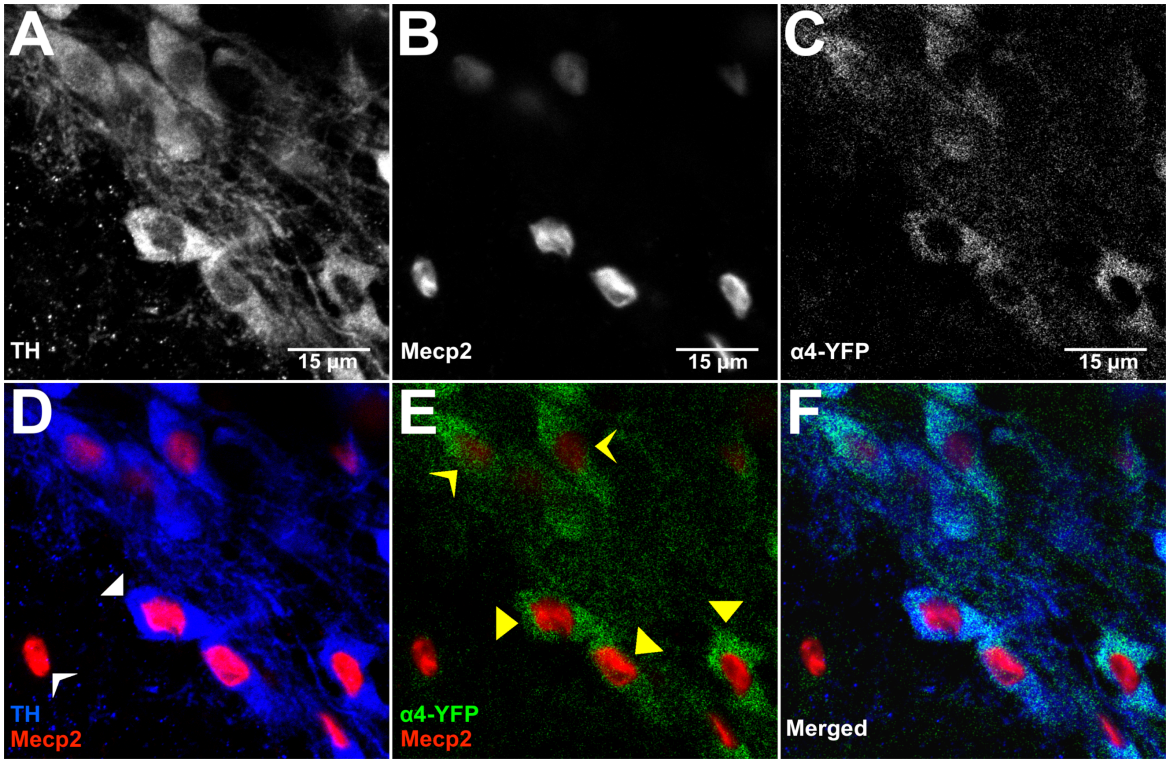

Figure 9. MeCP2 antibody labeling shows endogenous α4-YFP expression in mutant and wildtype DAergic cells in the SNc of a five-week-old Rett α4-YFP female mouse. **A-F**. Immunohistochemical labeling showing DAergic (TH, **A**) neurons of the SNC with mutant and Wt (MeCP2 antibody, **B**) MeCP2 proteins and endogenous α4-YFP (**C**) expression. **D**. Composite overlap showing specific TH labeling of DAergic neurons. Full white arrow shows a DAergic (TH-positive) cell. Slant white arrow shows a TH-negative cell from the SNr. **E**. Composite overlap showing α4-YFP expression on mutant and wildtype (Wt) DAergic neurons. Full yellow arrows show Wt (*Mecp2*$^{+}$) cells. Slant yellow arrow show mutant (*Mecp2*$^{-}$) cells. **F**. Composite overlap showing difference in spatial expression of α4-YFP on mutant and Wt DAergic neurons of the SNc of a P35 α4-YFP Rett female mouse (n = 1).

The TH labeling showed no difference in soma size between mutant and wildtype DAergic SNc neurons in the Rett female, and DAergic SNc neurons in wildtype female mice ($p = 0.036$, $F = 3.40$, $df = 2$, one-way anova; Mutant Rett-Wt Rett adj. $p = 0.99$, Mutant Rett-Wt adjusted $p = 0.071$, Wt Rett-Wt adjusted $p = 0.063$, Tukey HSD post-hoc tests) (Fig. 10A).

Mutant DAergic cells showed a 40% reduction in α4 nAChR subunit expression compared to their Wt counterparts in the Rett female ($p = 1.3 \times 10^{-6}$, $t = 5.2$, $df = 84$, Welch two sample t-test) and in the Wt females mice ($p = 7.6 \times 10^{-4}$, $t = 3.53$, $df = 66$, Welch two sample t-test) for the entire SNc region (Fig. 9B). However, no difference in levels of nAChR expression was found between the wild-type DAergic cells of the Rett and Wt female mice ($p = 0.67$, $t = 0.43$, $df = 81$, Welch two sample t-test) (Fig. 9B).

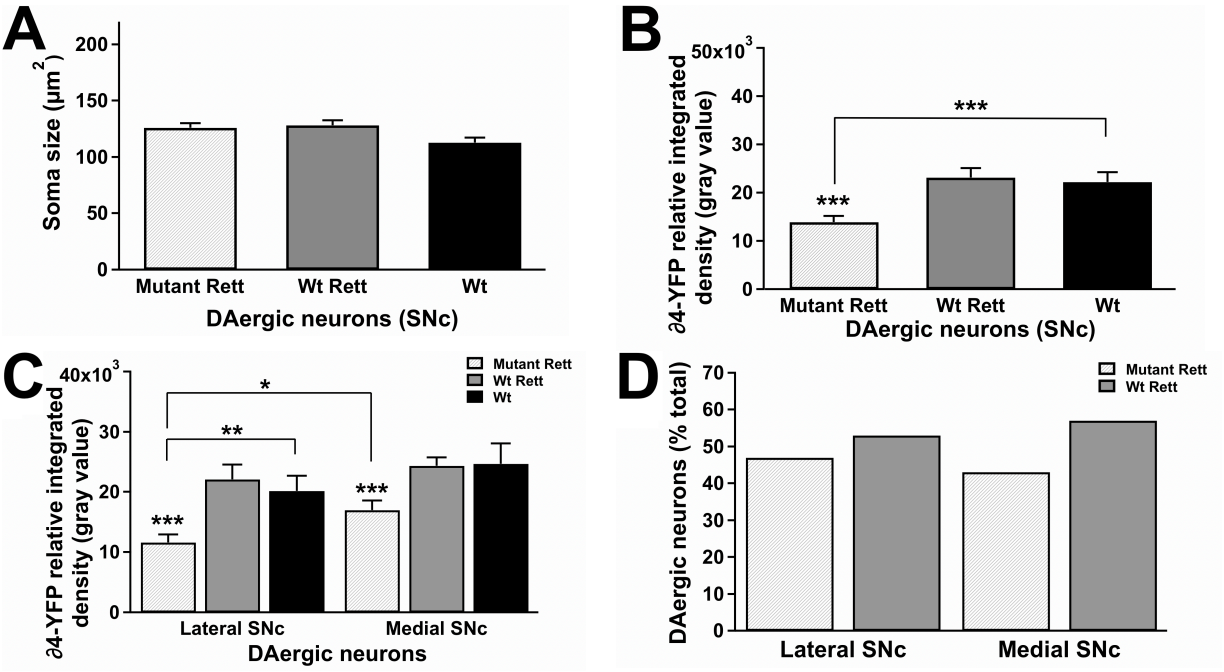

Figure 10. Mutant SNc DAergic neurons have a cell-autonomous reduction in α4* nAChR expression in a five-week-old Rett α4-YFP female mouse. **A**. TH labeling of the cell bodies of SNc DAergic neurons shows no statistical difference in soma size between mutant (n = 40) and Wt (n = 49) DAergic neurons of an α4-YFP Rett female mouse, and Wt (n = 46) DAergic neurons of α4-YFP Wt mice (p = 0.036, F = 3.40, df = 2, one way anova; Mutant Rett-Wt Rett adj. p = 0.99, Mutant Rett-Wt adj. p = 0.071, Wt Rett-Wt adj. p = 0.063, Tukey HSD post-hoc tests). **B**. Mutant SNc DAergic neurons have reduced α4 nAChR subunit expression, measured as relative integrated fluorescence density (arbitrary units), compared to Wt DAergic neurons in a P35 α4-YFP Rett female mouse ($p = 1.3x10^{-6}$, t = 5.2, df = 84, Welch two sample t-test) and Wt DAergic neurons in P35 Wt α4-YFP female mice ($p = 7.6x10^{-4}$, t = 3.53, df = 66, Welch two sample t-test). However, there is no difference in α4* nAChR expression in Wt DAergic neurons between P35 Rett and Wt female mice (p = 0.67, t = 0.43, df = 81, Welch two sample t-test). **C**. Mutant DAergic neurons show greater reduction in α4 nAChR subunit expression in the lateral SNc (n = 23) compared to the medial SNc (n = 17) (p = 0.013, W = 105, Wilcoxon rank-sum test). Within the lateral SNc, mutant DAergic neurons show greater reduction in α4 nAChR subunit expression compared their Wt DAergic counterparts in the Rett (n = 26) and Wt (n = 25) female mice (Rett female, $p = 8.2x10^{-4}$, W = 136, Wilcoxon rank-sum test; Wt females, p = 0.0069, W = 158, Wilcoxon rank-sum test). However, there is difference in α4* nAChR expression in Wt DAergic neurons between P35 Rett and Wt female mice in the lateral SNc (p = 0.45, W = 366, Wilcoxon rank-sum test). Within the medial SNc, Mutant DAergic neurons show greater reduction in α4 nAChR subunit expression compared their Wt DAergic counterparts in the Rett female (n =23) ($p = 6.7x10^{-4}$, W = 75, Wilcoxon rank-sum test). **D**. Distribution of mutant and Wt DAergic cells surveyed in the SNc of the Rett female mouse. Overall, there was a greater number of Wt DAergic cells (lateral SNc = 54%; medial SNc = 57%). All n values expressed as a number of cells taken from P35 $\alpha4^{YFP/+}$ female mice (n =3, 1 Rett, 2 wildtypes). *: indicates p < .05; **: indicates p < .01; ***: indicates p < .001.

A 30 % reduction in α4* nAChR expression was also found between mutant DAergic cells from the lateral SNc and mutant DAergic cells from the medial SNc ($p = 0.013$, $W = 105$, Wilcoxon rank-sum test) while levels of α4 nAChR subunit expression for Wt DAergic cells were similar across the lateral and medial SNc for both Rett and Wt female mice (Rett female, $p = 8.2 \times 10^{-4}$, $W = 136$, Wilcoxon rank-sum test; Wt females, $p = 0.0069$, $W = 158$, Wilcoxon rank-sum test) (Fig. 9C).

Finally, there was a greater number of Wt DAergic cells (lateral SNc = 54%; medial SNc = 57%) compared to their mutant counterparts (lateral SNc = 46%; medial SNc = 43% in the substantia nigra pars compacta of the Rett female (Fig. 9D).

Chapter 5 – Anatomical Findings Provide Evidence for Cholinergic Hypofunction in a Female RTT Mouse Model

5.1 Summary

The present study investigated if mutant DAergic cells have downregulated α4* nAChR expression compared to Wt DAergic cells in the SNc of a pre-symptomatic RTT female mouse and whether this downregulation was cell-autonomous. In order to perform the study, we implemented two crossbreeding strategies: one was meant to assess the validity of the experimental approach using female offspring heterozygous for $Mecp2^{EGFP}$ and $\alpha4^{YFP}$; the other was meant to test the research hypothesis using five-week-old RTT and wildtype female mice heterozygous for $\alpha4^{YFP}$. Following the therapeutic focus on human RTT female patients and the inherent advantages of X-inactivation for any research paradigm (within-subject design), only P35 female mice were analyzed in the study. Spectral confocal imaging was used to quantify the YFP-tagged α4* nAChRs in both types of mouse crossbreeds: it was first used to see whether the experimental approach was reliable by testing whether it was capable of spectrally unmix overlapping EGFP and YFP signals in the $Mecp2^{EGFP/+}$ crossbreeds; then, once the experimental approach was proven to be robust and accurate, it was used to quantify the α4-YFP signal between mutant and wildtype DAergic SNc cells in a RTT female mouse, and also in DAergic SNc cells of wildtype female mice. For five-week-old $Mecp2^{EGFP/+}/\alpha4^{YFP/+}$ mice, results showed that the α4 nAChR subunit expression in the medial habenula was much greater than in the medial perforant path. Furthermore, no difference in α4 nAChR subunit expression levels was found between $EGFP^+$ and $EGFP^-$ DAergic SNc neurons despite the spectral and spatial overlap of the YFP and EGFP signals. Finally, EGFP-positive and EGFP-negative DAergic SNc cells showed similar soma sizes. For the five-week-old RTT female mouse, results showed that mutant DAergic SNc neurons had downregulated α4 nAChR subunit expression compared to their Wt counterparts; moreover, this effect was found to be cell autonomous with the Wt DAergic SNc neurons of the RTT female mouse and the DAergic SNc neurons of Wt female mice showing similar levels of α4 nAChR subunit expression. The downregulation in nAChR expression found in mutant dopaminergic cells demonstrated subregion-specific effects with the mutant DAergic cells from the lateral SNc being more downregulated than the mutant DAergic cells from the medial SNc. This effect was specific to the mutant cells since no Wt DAergic cell populations from either the RTT female or her healthy sisters had different α4 nAChR subunit expression levels between the lateral and medial SNc.

All DAergic cells from all animals had similar soma sizes; however, in terms of cell number, the RTT female had less mutant DAergic cells than Wt cells.

5.2 Discussion

Consistent with results from previous studies examining the amount and upregulation of α4β2 nAChR in the medial habenula (MHb) and in the medial perforant pathway, Wt female mice had significantly more density of nicotinic receptors in cholinergic MHb neurons than in glutamatergic projections found in the medial perforant path (Nashmi et al., 2007; Renda and Nashmi, 2014). However, since the dynamics of receptor upregulation/downregulation were not considered in this study, we did not test whether these two brain regions had different amounts of receptor upregulation following chronic administration of nicotine, an exogenous agonist of nAChRs. Finally, the expression pattern of α4 nAChR subunits in the medial habenula was similar to that found in a previous study by Shih et al. (2014) which reported a ventrolateral gradient in the expression of α4- and β2-containing ACh receptors in MHb cholinergic neurons.

Spectral confocal imaging was also used to quantify the α4-YFP signal between EGFP-positive and EGFP-negative DAergic neurons in the SNc of young knock-in mouse crossbreeds. By unmixing the endogenous YFP and EGFP signals in healthy neurons, I was able to isolate a precise signal pertaining to the amount of α4 nAChR subunits on neuronal soma of individual cells. The data yielded findings that concurred with laboratory research describing the physical and behavioral phenotypes of MeCP2-EGFP knock-in mice as normal (Chahrour et al., 2008). Indeed, both DAergic neuron populations displayed similar soma sizes and amounts of α4* nAChRs for the substantia nigra pars compacta. The consequences of this result were two-fold: first, it strengthened the study's confidence on the wildtype characteristics of the *Mecp2*$^{EGFP/+}$ crossbreeds by showing that insertion of an EGFP sequence in the 3'UTR region of the *mecp2* gene did not affect cell size nor α4* receptor expression in DA neurons of the SNc; second, it validated the experimental approach of the study by demonstrating that (1) we could spectrally unmix spatially and spectrally overlapping EGFP and YFP signals at a subcellular levels and (2) that we were able to precisely quantify the amount of α4 nAChR subunits on individual cells. Following confirmation that the experimental method was robust and accurate, it led to another additional investigation of the consequences of MeCP2 loss-of-function in DA neurons of the SNc using a five-week-old RTT female mouse.

Results showed that mutant (*Mecp2*$^{-}$) DAergic neurons had reduced expression of α4* nAChRs compared to spatially colocalized Wt (*Mecp2*$^{+}$) DAergic neurons in the SNc of a young RTT female mouse. Furthermore, the reduction in nAChR expression in DAergic neurons was found to be cell-autonomous with Wt DAergic neurons from the RTT female and DAergic neurons from Wt females displaying similar amounts of α4* nAChRs on their soma. Finally, there was convincing evidence for differential brain regional reduction in nAChR expression in mutant DAergic neurons with the lateral SNc showing a greater reduction in levels of nAChR expression as compared to the medial SNc. To our knowledge, this is the first study to provide anatomical evidence for a cell-autonomous downregulation of α4 nAChR subunit expression in DAergic neurons in the SNc of a young RTT female mouse. These findings provide a bridge between recent results from behavioral research on RTT syndrome, and electrophysiological discoveries on cholinergic-modulated dopaminergic excitability and locomotion in the mouse substantia nigra (Leung et al., 2017; Estakhr et al., 2017).

First, the reduction in the amount of α4* nAChRs in mutant DAergic cells in the SNc might explain the behavioral variability associated with RTT female mice when subjected to acute injection of the α4/α6 agonist TC-2559 (Leung et al., 2017). Indeed, this reduction in α4 nAChRs subunits in mutant DA cell is relative to the amounts of nicotinic receptors in the colocalized Wt DA neurons. As such, individual variability in the absolute levels of nAChR expression could depend on the symptomatology of RTT syndrome in an all-or-none fashion: the modulatory role of the cholinergic inputs onto DAergic SNc neurons could be at full potential within a normal range of α4ß2 nAChR expression on DAergic neurons and only become impaired when amounts of α4ß2 nAChRs fall below that range. Furthermore, the increased downregulation of DAergic neurons from the lateral SNc compared to the medial SNc implicates regional effects of MeCP2 loss-of function that had been hypothesized in previous research (Oginsky et al., 2014; Leung et al., 2017). It also concurs with recent electrophysiological findings from Estakhr et al. (2017) reporting a differential effect of cholinergic inputs onto the SNc. In the study, cholinergic neurotransmission was found to enhance locomotion following lateral SNc DAergic neuron activation while medial SNc DAergic neurons receiving cholinergic-mediated GABAergic inputs supressed locomotor responses in mice. Following this model, a relative and region-specific decrease in amounts of α4ß2 nAChRs in the SNc of RTT female mice would indicate an overall motor suppressive effect of cholinergic neurotransmission on DAergic neurons that would be milder than the suppression of motor responses in Wt animals.

Recent behavioral data by Leung et al. (2017) strengthens the implications of this model with RTT female open-field movements following TC-2559 injection showing a locomotor suppression that was half of that seen in wildtype mice.

The ratio of mutant to Wt DA neurons in the SNc of the RTT female mouse resulting from X-chromosome inactivation (XCI) was similar to that found in previous studies examining neuronal distribution and dendritic morphologies in RTT mouse models (Dragich et al., 2000; Rietveld et al., 2015). The ratio was skewed in favour of Wt cells over mutant cells, which correlates with a greater ability for Wt cells to undergo cell division compared to mutant cells (Young and Zoghbi, 2004; Rietveld et al., 2015). While research reports that the majority of patients with RTT do have balanced XCI ratios, the likelihood of skewed XCI ratios is nonetheless greater in patients with X-linked disorders (Puck and Willard, 1998; Brown and Robinson, 2000; Shabazian et al., 2002).

Antibody labelling of neuronal cell body size of mutant and Wt DA neurons in the SNc of RTT and Wt female mice did not suggest any reduction in soma size for mutant DAergic cells compared to Wt cells, as evidenced in other studies (Bauman et al., 1995; Chen et al., 2001; Rietveld et al., 2015). However, such an effect might be age-dependent in terms of RTT symptomatology and also might show regional specificity. As a consequence, further experiments are needed to properly evaluate the presence or absence of differences in cell body size for both pre-symptomatic (younger than 3 months old) and symptomatic (older than 3 months old) RTT female mice.

Limitations for the study included: (1) the small sample size of RTT females, (2) the age of the offspring, (3) the time commitment for the staining and imaging protocols, and (4) the variability in the MeCP2 histochemical labeling. First, due to the limited breeding of RTT mice and the low survival rate of RTT litters, I was only able to investigate differences of α4 nAChR subunit expression between mutant and Wt DAergic neurons in a single RTT female mouse. Considering the low variability of the data, two or three RTT female would have been sufficient to strengthen the results outlined in this study. Second, the inherent limitations of the study's timeline prevented a thorough investigation of age-dependent effects of RTT syndrome in female mice with regards to nAChR expression of DAergic neurons of the SNc. The gradual onset of the RTT phenotype in human patients and mouse models can create differential changes in the alteration of CNS neurotransmitter systems throughout the lifespan of a RTT carrier.

Therefore, it would be beneficial to the study to further investigate levels of nAChR expression in DA neurons of the SNc for fully symptomatic RTT female mice in order to fully characterize the consequences of MeCP2 loss-of function on the functionality of the cholinergic system. Third, revisions must be made to the experimental approach to reduce the time necessary of the processing and imaging of brain sections. Finally, corrections to the perfusion protocol must be applied in order to test whether one can obtain a better labeling of the MeCP2 protein which would facilitate the distinction between mutant and Wt cells.

5.3 *Future Directions*

Based on the data, the primary goal of future experiments would be to replicate the study's results with a greater number of RTT female mice. Experiments would also be repeated over different brain regions and neuron subtypes that are known to have cholinergic inputs -such as the medial prefrontal cortex (med. PFC), the hippocampus, the thalamus, the VTA, the SNr- as well as in different age groups, with both young and old female mice. This would allow us to examine whether dysregulation of the cholinergic system is ubiquitous in the mouse CNS as a consequence of RTT.

Future research would also benefit from investigating whether this dysregulation of nAChR expression in the SNc can be dynamically modulated by chronic administration of pharmacological agents in RTT female mice. Considering the reversibility of MeCP2 dysfunction, these experiments could provide potential therapeutic axes for the treatment of RTT in human patients.

Chapter 6 – Appendix

Table 1.
Soma size of dopaminergic SNc neurons as a function of the female mouse *Mecp2* genotype

Mecp2 genotype	Soma size (μm^2)	Sample size (n)
Mecp2EGFP^{+}	127.0 ± 3.8	54
Mecp2EGFP^{-}	131.9 ± 4.2	48
Mecp2^{-}	126.0 ± 3.9	40
Mecp2^{+} (RTT)	128.2 ± 4.6	49
Mecp2^{+} (Wt)	112.6 ± 4.3	46

Values are reported as mean ± S.E.M and rounded to the first decimal. All n values are expressed as a number of cells taken from P35 female mice (n = 5, 2 *Mecp2EGFP*$^{+/-}$/ *α4YFP*$^{+/-}$ mice, 1 *Mecp2*$^{+/-}$ /*α4YFP*$^{+/-}$ mouse (RTT), 2 *α4YFP*$^{+/-}$ mice)

Table 2.
α4YFP fluorescence density levels in dopaminergic SNc neurons as a function of the female mouse *Mecp2* genotype

Mecp2 genotype	Mean α4YFP integrated density	Sample size (n)
Mecp2EGFP^{+}	23537.7 ± 1599	54
Mecp2EGFP^{-}	25884.8 ± 1394	48
Mecp2^{-}	13891.3 ± 1273	40
Mecp2^{+} *(RTT)*	23133.3 ± 1935	49
Mecp2^{+} *(Wt)*	22204.4 ± 2044	46

Values are reported as mean ± S.E.M and rounded to the first decimal. All n values are expressed as a number of cells taken from P35 female mice (n = 5, 2 *Mecp2EGFP*$^{+/-}$/ *α4YFP*$^{+/-}$ mice, 1 *Mecp2*$^{+/-}$/ *α4YFP*$^{+/-}$ mouse (RTT), 2 *α4YFP*$^{+/-}$ mice)

Table 3.
α4YFP fluorescence density levels in dopaminergic neurons between mouse *Mecp2* genotypes in lateral and medial SNc

Mecp2 genotype	Mean α4YFP integrated density		Sample size (n)	
	Medial SNc	Lateral SNc	Medial SNc	Lateral SNc
Mecp2^{-}	16989.3 ± 1585.3	11601.4 ± 1342.9	17	23
Mecp2^{+} *(RTT)*	24330.4 ± 1406.7	22074.3 ± 2449.6	23	26
Mecp2^{+} *(Wt)*	24645.8 ± 3377.3	20153.6 ± 2524.3	21	25

Values are reported as mean ± S.E.M and rounded to the first decimal. All n values are expressed as a number of cells taken from P35 female mice (n = 3, 1 *Mecp2*$^{+/-}$/ *α4YFP*$^{+/-}$ mouse (RTT), 2 *α4YFP*$^{+/-}$ mice)

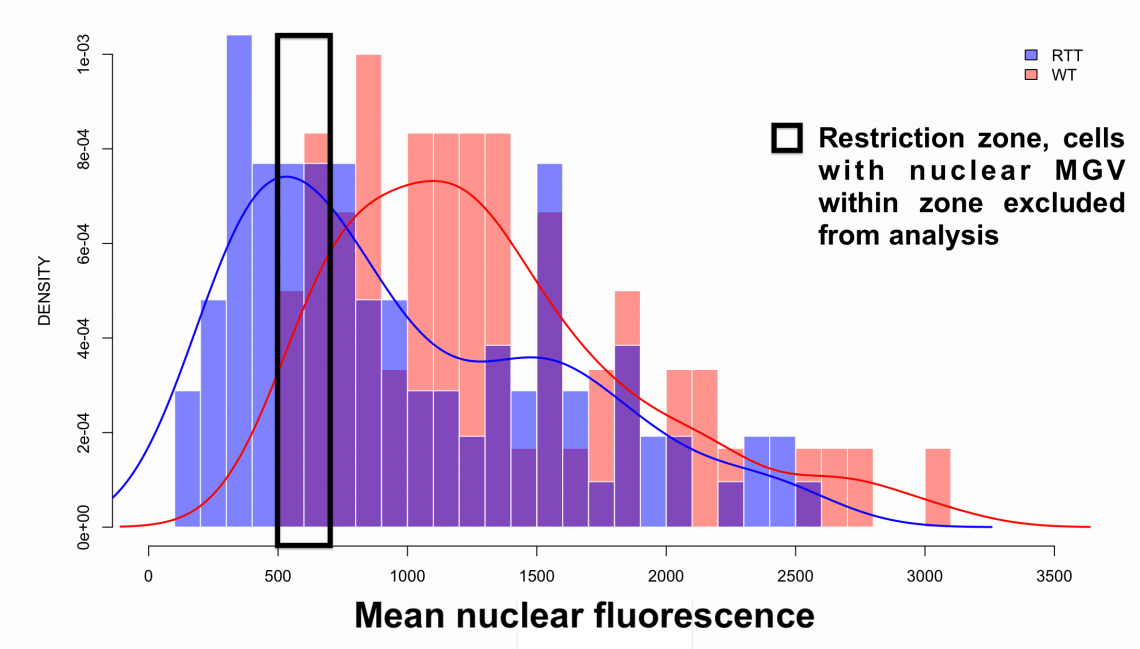

Figure 11. Overlapping frequency distribution of DAergic SNC neurons as a function of the nuclear fluorescence mean gray value in P35 $\alpha 4^{YFP/+}$ wild-type *and* RTT female mice. A restriction zone was implemented as a function of the characteristic distributions of the nuclear mean gray values between the two mouse phenotypes and was used to separate mutant from wild-type neurons in the RTT female mouse.

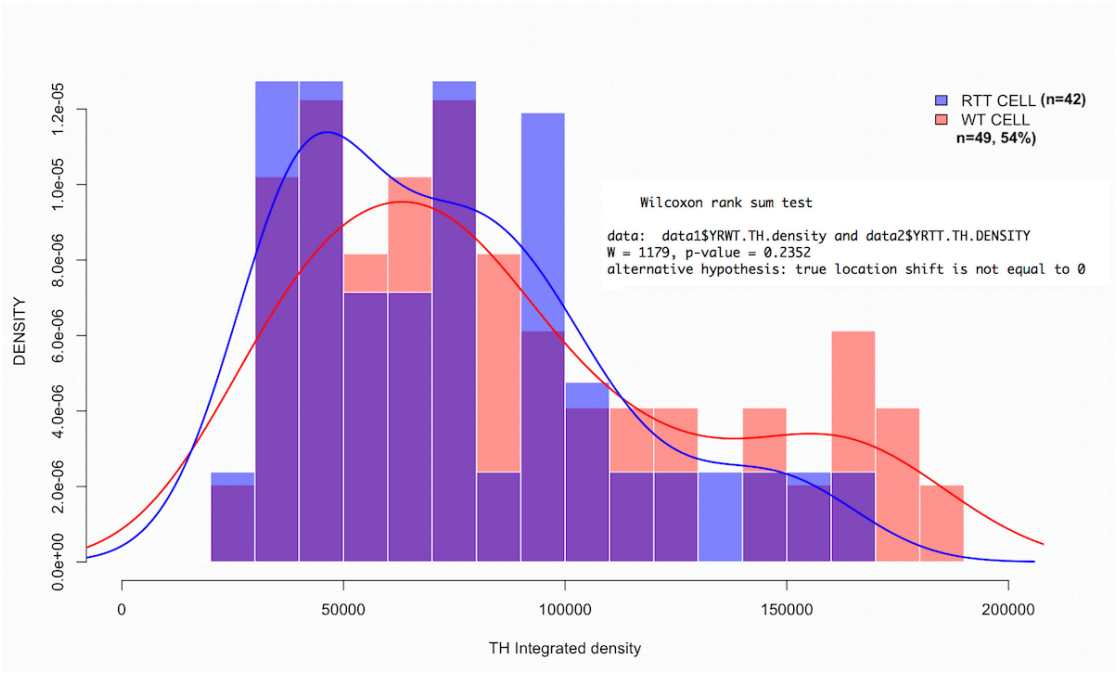

Figure 12. Overlapping frequency distribution of mutant and wild-type DAergic SNC neurons as a function of the relative tyrosine hydroxylase fluorescence density in a P35 $\alpha 4^{YFP/+}$ RTT female mouse.

Chapter 7 - Bibliography

Albuquerque E.X., Pereira E.F., Mike A., Eisenberg H.M., Maelicke A., and Alkondon M. (2000). Neuronal nicotinic receptors in synaptic functions in humans and rats: physiological and clinical relevance. Behav. Brain Res. *113*,131–141.

Amir, R.E., Van den Veyver, I.B., Wan, M., Tran, C.Q., Francke, U., and Zoghbi, H.Y. (1999). Rett syndrome is caused by mutations in X-linked MECP2, encoding methyl-CpG-binding protein 2. Nat. Genet. *23*, 185– 188.

Anden, N.-E., Dahlstrom, A., Fuxe, K., Larsson, K., Olson, K., and Ungerstedt, U. (1966). Ascending monoamine neurons to the telencephalon and diencephalon. Acta Physiol. Scand. *67*, 313-326

Araque A., Martín E.D., Perea G., Arellano J.I., and Buño W. (2002). Synaptically released acetylcholine evokes Ca2+ elevations in astrocytes in hippocampal slices. J. Neurosci. *22*, 2443–2450.

Archer, H.L., Whatley, S.D., Evans, J.C., Ravine, D., Huppke, P., Kerr, A., Bunyan, D., Kerr, B., Sweeney, E., Davies, S.J., et al. (2006b). Gross rearrangements of the MECP2 gene are found in both classical and atypical Rett syndrome patients. J. Med. Genet. *43*, 451–456.

Asaka, Y., Jugloff, D.G., Zhang, L., Eubanks, J.H., and Fitzsimonds,R.M. (2006). Hippocampal synaptic plasticity is impaired in the Mecp2-null mouse model of Rett syndrome. Neurobiol. Dis. *21*, 217–227.

Bauman M.L., Kemper T.L., and Arin D.M. (1995). Pervasive neuroanatomic abnormalities of the brain in three cases of Rett's syndrome. Neurol. *45*, 1581-86.

Bateup, H. S., Santini, E., Shen, W., Birnbaum, S., Valjent, E., Surmeier, D. J., . . . Greengard, P. (2010). Distinct subclasses of medium spiny neurons differentially regulate striatal motor behaviors. Proc. Nat. Aca. Sci. USA*, 107*, 14845-14850.

Bourdon, V., Philippe, C., Bienvenu, T., Koenig, B., Tardieu, M., Chelly, J., and Jonveaux, P. (2001). Evidence of somatic mosaicism for a MECP2 mutation in females with Rett syndrome: diagnostic implications. J. Med. Genet. *38*, 867–871.

Brown C.J. and Robinson W.P. (2000). The causes and consequences of random and non-random X chromosome inactivation in humans. Clin Genet *58*, 353-363.

Buisson B. and Bertrand D. (2001). Chronic exposure to nicotine upregulates the human (alpha)4((beta)2 nicotinic acetylcholine receptor function. J. Neurosci. *21*,1819–1829.

Chahrour, M., Jung, S. Y., Shaw, C., Zhou, X., Stephen T. C. Wong, Qin, J., and Zoghbi, H. Y. (2008). MeCP2, a key contributor to neurological disease, activates and represses transcription. *Sci. 320*, 1224-1229.

Chahrour, M., and Zoghbi, H. Y. (2007). The story of Rett syndrome: From clinic to neurobiology. Neuron*, 56*, 422-437.

Chao, H., Zoghbi, H.Y., and Rosenmund, C. (2007). MeCP2 controls excitatory synaptic strength by regulating glutamatergic synapse number. Neuron *56*, 1–8.

Cheer J.F., Wassum K.M., Sombers L., Heien M.L., Ariansen J.L., Aragona B.J., Phillips P.E.M., and Wightman R.M. (2007). Phasic dopamine release evoked by abused substances requires cannabinoid receptor activation. J. Neurosci.: Of. J. Soc. Neurosci. *27*:791–795.

Chen, R.Z., Akbarian, S., Tudor, M., and Jaenisch, R. (2001). Deficiency of methyl-CpG binding protein-2 in CNS neurons results in a Rett-like phenotype in mice. Nat. Genet. *27*, 327–331.

Christodoulou, J., Grimm, A., Maher, T., and Bennetts, B. (2003). Re- ttBASE: The IRSA MECP2 variation database-a new mutation data- base in evolution. Hum. Mutat. *21*, 466–472.

Clarke, P.B., Hommer, D.W., Pert, A., and Skirboll, L.R. (1987). Innervation of substantia nigra neurons by cholinergic afferents from pedunculopontine nucleus in the rat: neuroanatomical and electrophysiological evidence. Neurosci. *23*, 1011–1019.

Cornwall, J., Cooper, J.D., and Phillipson, O.T. (1990). Afferent and efferent connections of the laterodorsal tegmental nucleus in the rat. Brain Res. Bull. *25*, 271–284.

Dani, V.S., Chang, Q., Maffei, A., Turrigiano, G.G., Jaenisch, R., and Nelson, S.B. (2005). Reduced cortical activity due to a shift in the balance between excitation and inhibition in a mouse model of Rett syndrome. Proc. Natl. Acad. Sci. USA *102*, 12560–12565.

Dragich, J., Houwink-Manville, I., and Schanen, C. (2000). Rett syndrome: a surprising result of mutation in MECP2. Hum. Mol. Genet. *9*, 2365–2375.

Dragich, J.M., Kim, Y.H., Arnold, A.P., and Schanen, N.C. (2007). Differential distribution of the MeCP2 splice variants in the postnatal mouse brain. J. Comp. Neurol. *501*, 526–54.

Estakhr J., Abazari D., Frisby K., McIntosh J. M., and Nashmi R. (2017). Differential control of dopaminergic excitability and locomotion by cholinergic inputs in mouse substantia nigra. Curr. Biol. *13*, 1900-1914

Gemelli, T., Berton, O., Nelson, E.D., Perrotti, L.I., Jaenisch, R., and Monteggia, L.M. (2006). Postnatal loss of methyl-CpG binding protein 2 in the forebrain is sufficient to mediate behavioral aspects of Rett syndrome in mice. Biol. Psychiatry *59*, 468–476.

Gerfen, C.R., Engber, T.M., Mahan, L.C., Susel, Z., Chase, T.N., Monsma, F.J., Jr., and Sibley, D.R. (1990). D1 and D2 dopamine receptor-regulated gene expression of striatonigral and striatopallidal neurons. Sci. *250*, 1429– 1432.

Gerfen, C. R., and Wilson, C. J. (1996). The Basal ganglia. Handbook of chemical neuroanatomy, L. W. Swanson, A. Björklund and T. Hokfelt (eds.). Vol. 12: Int. Sys. CNS, Part III. New York: Raven Press, 427-504

Gioanni Y., Rougeot C., Clarke P.B., Lepousé C., Thierry M., and Vidal C. (1999) Nicotinic receptors in the rat prefrontal cortex: increase in glutamate release and facilitation of mediodorsal thalamo-cortical transmission. Eur. J. Neurosci. *11*,18–30.

Grillner, S., Hellgren, J., Ménard, A., Saitoh, K., and Wikström, M. A. (2005). Mechanisms for selection of basic motor programs: Roles for the striatum and the pallidum. Trends Neurosci. *28*, 364-370

Guy, J., Hendrich, B., Holmes, M., Martin, J.E., and Bird, A. (2001). A mouse Mecp2-null mutation causes neurological symptoms that mimic Rett syndrome. Nat. Genet. *27*, 322–326.

Guy, J., Gan, J., Selfridge, J., Cobb, S., and Bird, A. (2007). Reversal of neurological defects in a mouse model of Rett syndrome. Sci. *315*,1143–1147.

Hagberg, B., Aicardi, J., Dias, K., and Ramos, O. (1983). A progressive syndrome of autism, dementia, ataxia, and loss of purposeful hand use in girls: Rett's syndrome: report of 35 cases. Ann. Neurol. *14*, 471–479.

Hagberg, B. (2005). Rett syndrome: long-term clinical follow-up experiences over four decades. J. Child Neurol. *20*, 722–727.

Hendrich, B., and Bird, A. (1998). Identification and characterization of a family of mammalian methyl-CpG binding proteins. Mol. Cell. Biol. *18*, 6538–6547.

Henneman, E. (1990). Comments on the logical basis of muscle control. *Segmental Motor System,* M. C. Binder and L. M. Mendell (eds.). New York: Oxford University Press, 7-10

Hansen, S. B., Taylor, P., Sulzenbacher, G., Bourne, Y., Huxford, T., and Marchot, P. (2005). Structures of aplysia AChBP complexes with nicotinic agonists and antagonists reveal distinctive binding interfaces and conformations. EMBO J. *24*, 3635-3646.

Jian, L., Nagarajan, L., de Klerk, N., Ravine, D., Bower, C., Anderson, A., Williamson, S., Christodoulou, J., and Leonard, H. (2006). Predictors of seizure onset in Rett syndrome. J. Pediatr. *149*, 542–547.

Jung, B.P., Jugloff, D.G., Zhang, G., Logan, R., Brown, S., and Eubanks, J.H. (2003). The expression of methyl CpG binding factor MeCP2 correlates with cellular differentiation in the developing rat brain and in cultured cells. J. Neurobiol. *55*, 86–96.

Kaji, R. (2001). Basal ganglia as a sensory gating device for motor control. J. Med. Invest. *48*, 142-146

Kemp, J. M., and Powell, T. P. S. (1970). The cortico-striate projection in the monkey. Brain *93*, 525-546

Kenny P.J., File S.E., Neal M.J. (2000). Evidence for a complex influence of nicotinic acetylcholine receptors on hippocampal serotonin release. Journal of neurochemistry *75*, 2409–2414.

Kocsis, J. D., Sugimori, M., and Kitai, S. T. (1977). Convergence of excitatory synaptic inputs to caudate spiny neurons. Brain Res. 124: 403-413

Kriaucionis, S. and Bird, A. (2004). The major form of MeCP2 has a novel N-terminus generated by alternative splicing. Nucleic Acids Res. *32*, 1818–1823.

Larson, J. M. (2006). The nikon C1si combines high spectral resolution, high sensitivity, and high acquisition speed. Cytometry *69A,* 825-834.

Laviolette S.R., van der Kooy D. (2004). The neurobiology of nicotine addiction: bridging the gap from molecules to behaviour. Nat. Rev. Neurosci. 5,55–65.

Léna C., Changeux J. (1997). Role of Ca2+ ions in nicotinic facilitation of GABA release in mouse thalamus. The Journal of neuroscience 17:576–585.

Léna C., Changeux J., and Mulle C. (1993). Evidence for “preterminal” nicotinic receptors on GABAergic axons in the rat interpeduncular nucleus. J. Neurosci. *13*, 2680–2688.

Leung, J., McPhee, D., Renda, T., Penty, N., Farhoomand, F., Nashmi R., and Delaney, K. (2017). MeCP2-deficient mice have reduced α4 and α6 nicotinic receptor mRNA and altered behavioral response to nicotinic agonists. Behav. Brain Res. *330*, 118-126

Li X., Eisenach J.C. (2002). Nicotinic acetylcholine receptor regulation of spinal norepinephrine release. Anesthesiology *96*, 1450–1456.

Li, M. D. (2016). *Nicotinic acetylcholine receptor technologies*. New York: Humana Press.

Luikenhuis, S., Giacometti, E., Beard, C.F., and Jaenisch, R. (2004). Expression of MeCP2 in postmitotic neurons rescues Rett syndrome in mice. Proc. Natl. Acad. Sci. USA *101*, 6033–6038.

Lundberg, A. (1975). Control of spinal mechanisms from the brain. *The Nervous System*, Volume 1: *The Basic Neurosciences*. D. B. Tower (ed.). New York: Raven Press, pp. 253-265

Matarazzo, V., Cohen, D., Palmer, A.M., Simpson, P.J., Khokhar, B., Pan, S.J., and Ronnett, G.V. (2004). The transcriptional repressor Mecp2 regulates terminal neuronal differentiation. Mol. Cell. Neurosci. *27*, 44–58.

Matsumura, M., Watanabe, K., and Ohye, C. (1997). Single-unit activity in the primate nucleus tegmenti pedunculopontinus related to voluntary arm movement. Neurosci. Res. *28*, 155–165.

Martinowich, K., Hattori, D., Wu, H., Fouse, S., He, F., Hu, Y., Fan, G., and Sun, Y.E. (2003). DNA methylation-related chromatin remodeling in activity-dependent BDNF gene regulation. Science *302*, 890–893.

McCoy, A. N., and Tan, S. Y. (2014). Otto loewi (1873-1961): Dreamer and Nobel laureate. Singapore Med. J. *55*, 3.

McGill, B.E., Bundle, S.F., Yaylaoglu, M.B., Carson, J.P., Thaller, C., and Zoghbi, H.Y. (2006). Enhanced anxiety and stress-induced corti- costerone release are associated with increased Crh expression in a mouse model of Rett syndrome. Proc. Natl. Acad. Sci. USA *103*, 18267–18272.

Mink, J.W. (1996). The basal ganglia: focused selection and inhibition of competing motor programs. Prog. Neurobiol. *50*, 381–425.

Miyake, K., and Nagai, K. (2007). Phosphorylation of methyl-CpG binding protein 2 (MeCP2) regulates the intracellular localization during neuronal cell differentiation. Neurochem. Int. *50*, 264–270.

Moretti, P., Levenson, J.M., Battaglia, F., Atkinson, R., Teague, R., Antalffy,B., Armstrong, D., Arancio, O., Sweatt, J.D., and Zoghbi, H.Y. (2006). Learning and memory and synaptic plasticity are impaired ina mouse model of Rett syndrome. J. Neurosci. *26*, 319–327.

Nagai, T., Ibata, K., Park, E. S., Kubota, M., Mikoshiba, K., Miyawaki, A. (2002). A variant of yellow fluorescent protein with fast and efficient maturation for cell-biological applications. Nat. Biotech. *20,* 87–90.

Nakamura, K., and Hirosaka, O. (2006). Role of dopamine in the primate caudate nucleus in reward modulation of saccades. J. Neurosci. *26*:5360-5369

Nan, X., Campoy, F.J., and Bird, A. (1997). MeCP2 is a transcriptional repressor with abundant binding sites in genomic chromatin. Cell *88*, 471–481.

Nashmi R., and Lester H.A. (2006). CNS Localization of Neuronal Nicotinic Receptors. J. Mol. Neurosci. *30*, 181–184.

Nashmi, R., Xiao, C., Deshpande, P., McKinney, S., Grady, S. R., Whiteaker, P., . . . Lester, H. A. (2007). Chronic nicotine cell specifically upregulates functional alpha 4 nicotinic receptors: Basis for both tolerance in midbrain and enhanced long-term potentiation in perforant path. The J. Neurosci. *27*, 8202.

Nelson M.E., Kuryatov A., Choi C.H., Zhou Y., Lindstrom J. (2003). Alternate stoichiometries of alpha4beta2 nicotinic acetylcholine receptors. Mol. Pharma. *63*, 332–341.

Nelson, E.D., Kavalali, E.T., and Monteggia, L.M. (2006). MeCP2-dependenttranscriptional repression regulates excitatory neurotransmission. Curr. Biol. 16, 710–716.

Nikitina, T., Shi, X., Ghosh, R.P., Horowitz-Scherer, R.A., Hansen, J.C., and Woodcock, C.L. (2007). Multiple modes of interaction between the methylated DNA binding protein MeCP2 and chromatin. Mol. Cell. Biol. *27,* 864–877.

Norton, A.B.W., Jo, Y.S., Clark, E.W., Taylor, C.A., and Mizumori, S.J.Y. (2011). Independent neural coding of reward and movement by pedunculopontine tegmental nucleus neurons in freely navigating rats. Eur. J. Neurosci. *33*, 1885–1896.

Nuber, U.A., Kriaucionis, S., Roloff, T.C., Guy, J., Selfridge, J., Steinh- off, C., Schulz, R., Lipkowitz, B., Ropers, H.H., Holmes, M.C., and Bird, A. (2005). Upregulation of glucocorticoid-regulated genes in a mouse model of Rett syndrome. Hum. Mol. Genet. *14*, 2247–2256.

Oginsky, M.F., Cui N., Zhong W., Hohnson C.M., and Jiang C. (2014). Alterations in the cholinergic system of brain stem neurons in a mouse model of Rett syndrome. Am. J. Physiol. Cell Physiol. *307*, 508-528.

Pan, H., Li, M.R., Nelson, P., Bao, X.H., Wu, X.R., and Yu, S. (2006). Large deletions of the *MECP2* gene in Chinese patients with classical Rett syndrome. Clin. Genet. *70*, 418–419.

Puck J.M., and Willard H.F. (1998). X inactivation in females with X-linked disease. N. Engl. J. Med. *338*, 325-328.

Purves, D. (2018). *Neuroscience*. Sunderland, Mass: Sinauer Associates.

Ravn, K., Nielsen, J.B., Skjeldal, O.H., Kerr, A., Hulten, M., and Schwartz, M. (2005). Large genomic rearrangements in *MECP2*. Hum. Mutat. *25*, 324.

Redgrave P., Rodriguez M., Smith Y., Rodriguez-Oroz M. C., Lehericy S., Bergman H., Agid Y., DeLong M. R., and Obeso J.A. (2010). Goal-directed and habitual control in the basal ganglia: implications for Parkinson's disease. Nat. Rev. Neurosci. *11*, 760-772

Renda A., and Nashmi R. (2012). Spectral confocal imaging of fluorescently tagged nicotinic receptors in knock-in mice with chronic nicotine administration. J. Vis. Exp. *60*, 1–10.

Renda, A., and Nashmi, R. (2014). Chronic nicotine pretreatment is sufficient to upregulate α4 nicotinic receptors and increase oral nicotine self-administration in mice. BMC Neurosci. *15*, 89.

Renda, A., Penty, N., Komal, P., Nashmi, R. (2016). Vulnerability to nicotine self-administration in adolescent mice correlates with age-specific expression of α4* nicotinic receptors, Neuropharmacology *108*, 49-59.

Rett, A. (1966). Wien. Med. Wochenschr. *116*, 723–726

Rietveld, L., Stuss, D. P., McPhee, D., & Delaney, K. R. (2015). Genotype-specific effects of Mecp2 loss-of-function on morphology of layer V pyramidal neurons in heterozygous female Rett syndrome model mice. Front. Cell. Neurosci. *9*, 145.

Roerig B., Nelson D.A., Katz L.C., Carolina N. (1997). Fast Synaptic Signaling by Nicotinic Acetylcholine and Serotonin 5-HT 3 Receptors in Developing Visual Cortex. J. Neurosci. *17*,8353–8362.

Roze, E., Cochen, V., Sangla, S., Bienvenu, T., Roubergue, A., Leu-Se- menescu, S., and Vidaihet, M. (2007). Rett syndrome: An overlooked diagnosis in women with stereotypic hand movements, psychomotor retardation, Parkinsonism, and dystonia. Mov. Disord. *22*, 387–389.

Samaco, R.C., Hogart, A., and LaSalle, J.M. (2005). Epigenetic overlap in autism-spectrum neurodevelopmental disorders: MECP2 deficiency causes reduced expression of UBE3A and GABRB3. Hum. Mol. Genet. *14*, 483–492.

Shahbazian M.D., Antalffy B., Armstrong D.L. and Zoghbi H.Y. (2002) Insight into Rett syndrome: Mecp2 levels display tissue- and cell-specific differences and correlate with neuronal maturation. Hum. Mol. Genet. *11*, 115-24.

Shih, P., Engle, S. E., Oh, G., Deshpande, P., Puskar, N. L., Lester, H. A., and Drenan, R. M. (2014). Differential expression and function of nicotinic acetylcholine receptors in subdivisions of medial habenula. J. Neurosci. *34*, 9789

Singh, J., Saxena, A., Christodoulou, J., and Ravine D. (2008). *MECP2* genomic structure and function: Insights from ENCODE. Nucleic Acids Res. *36*, 6035-6047.

Smeets, E., Terhal, P., Casaer, P., Peters, A., Midro, A., Schollen, E., van Roozendaal, K., Moog, U., Matthijs, G., Herbergs, J., et al. (2005). Rett syndrome in females with CTS hot spot deletions: a disor- der profile. Am. J. Med. Genet. A. *132*, 117–120.

Smith, Y., Bevan, M. D., Shink, E. and Bolam, J. P. (1998). Microcircuitry of the indirect and direct pathways of the basal ganglia. Neurosci. *86*, 353-387.

Steg, G., and Johnels, B. (1994). Physiological mechanisms and movement analysis in Parkinson's disease. Mol. Neurobiol. *9*, 143-147.

Stuss D.P., Boyd J.D., Levin D.B., and Delaney K. R. (2012). Mecp2 Mutation Results in Compartment-Specific reductions in dendritic branching and spine density in Layer 5 Motor cortical neurons of YFP-H Mice. PLoS One *7*, e31896.

Tecuapetla, F., Jin, X., Lima, S. Q., and Costa, R. M. (2016). Complementary contributions of striatal projection pathways to action initiation and execution. Cell *166,* 703-715.

Thastrup O., Tullin S., Kongsbak Poulsen L., Bjørn S. (2001) Fluorescent Proteins,

Trappe, R., Laccone, F., Cobilanschi, J., Meins, M., Huppke, P., Hanefeld, F., and Engel, W. (2001). MECP2 mutations in sporadic cases of Rett syndrome are almost exclusively of paternal origin. Am. J. Hum. Genet. *68*, 1093–1101

Wan, M., Lee, S.S., Zhang, X., Houwink-Manville, I., Song, H.R., Amir, R.E., Budden, S., Naidu, S., Pereira, J.L., Lo, I.F., et al. (1999). Rett syndrome and beyond: recurrent spontaneous and familial *MECP2* mutations at CpG hotspots. Am. J. Hum. Genet. *65*, 1520–1529.

Wenk, G.L. (1997). Rett syndrome: neurobiological changes underlying specific symptoms. Prog Neurobiol. *51*,383–391.

Whiting P., and Lindstrom J. (1986). Pharmacological receptors properties of immuno-isolated neuronal nicotinic. J. Neurosci. *6*, 3061–3069.

Whiting I. P. J., Swanson L.W., and Simmons D. M. (1987). lmmunohistochemical localization of neuronal nicotinic receptors in the rodent central nervous system. J. Neurosci. *7*, 3334–3342.

Young J.I., and Zoghbi H. Y. (2004). X-chromosome inactivation patterns are unbalanced and affect the phenotypic outcome in a mouse model of rett syndrome. Am. J. Hum. Genet. *74*, 511-20.

Young, J.I., Hong, E.P., Castle, J.C., Crespo-Barreto, J., Bowman, A.B., Rose, M.F., Kang, D., Richman, R., Johnson, J.M., Berget, S., and Zoghbi, H.Y. (2005). Regulation of RNA splicing by the methylation-dependent transcriptional repressor methyl-CpG binding protein 2. Proc. Natl. Acad. Sci. USA *102*, 17551–17558.

Zachariah, R., and Rastegar M. (2012). Linking Epigenetics to Human Disease and Rett Syndrome: The Emerging Novel and Challenging Concepts in MeCP2 Research. Neural Plastic.

Zimmermann, T. (2005). Spectral imaging and linear unmixing in light microscopy. Berlin, Heidelberg: Springer Berlin Heidelberg. 245-26.